Synthesis of $CoSe_2$/RGO Composites and Their Application in a Counter Electrode of Dye-sensitized Solar Cells

Woo-Yeol Choi

Department of Chemical Engineering
Graduate School of UNIST

2015

Synthesis of $CoSe_2$/RGO Composites and Their Application in a Counter Electrode of Dye-sensitized Solar Cells

Woo-Yeol Choi

Department of Chemical Engineering
Graduate School of UNIST

Synthesis of $CoSe_2$/RGO Composites and Their Application in a Counter Electrode of Dye-sensitized Solar Cells

A thesis
submitted to the Graduate School of UNIST
in partial fulfillment of the
requirements for the degree of
Master of Science

Woo-Yeol Choi

12. 18. 2014
Approved by

Sung You Hong

Advisor
Sung You Hong

Synthesis of $CoSe_2$/RGO Composites and Their Application in a Counter Electrode of Dye-sensitized Solar Cells

Woo-Yeol Choi

This certifies that the thesis of Woo-Yeol Choi is approved.

12. 18. 2014

Thesis supervisor: Sung You Hong

Yongseok Jun

Tae-Hyuk Kwon

Abstract

Nowadays, the energy issues regarding to fossil fuels have become serious problems. Though fossil fuels such as coal, natural gas and petroleum are cheap and convenient to use, they have triggered the air pollution caused by the emission of harmful gas after burning them. To resolve these problems, the renewable energy can be a good option, which use eco-friendly resources such as sunlight, wind, water, and etc.

Solar cells have emerged as one of the promising renewable energy devices due to the usage of solar energy which can satisfy the future global need for renewable energy sources. After the development of single crystalline silicon-base solar cells that were the first solar cells, many types of solar cells have been extensively studied and researched to further improve efficiency and make up for the disadvantages. As such efforts, thin film solar cells such as CIGS and CdTe, and next-generation solar cells such as polymer solar cells have been developed for low-cost and high efficiency solar cells.

Dye-sensitized solar cells (DSSCs), one of the next-generation solar cells, have attracted great attention since Grätzel's group introduced them in 1991 first due to their easy fabrication and cost-effectiveness compared with silicon based solar cells. A typical DSSC comprises nanocrystalline titanium dioxide (TiO_2) films, dye molecules as light-senstizers, iodide (I^-) and triiodide (I_3^-) redox couple electrolyte, and platinum (Pt) electrocatalysts covered onto transparent conductive oxide (TCO). Among the parts of DSSCs, electrocatalyst materials play roles as the catalyst for reduction of I_3^- to I^- in the liquid-based electrolyte. Due to its superior catalytic effects for I_3^- reduction and chemical stability, Pt has been widely used as a counter electrode (CE) material in DSSCs. However, the scarcity of rare Pt metal severely makes fabrication cost of DSSCs high and hinders the large-scale production of DSSCs. Because of these reasons, finding more abundant and cheaper materials than Pt is necessary. In this study, cobalt diselenide ($CoSe_2$) and the composites of $CoSe_2$ and reduced graphene oxide ($CoSe_2$@RGO) were synthesized by a facile hydrothermal reaction of cobalt ions and selenide source with or without graphene oxide. Analyses with X-ray, Raman and morphology revealed the formation of $CoSe_2$ compounds and reduction of graphene oxide. Electrochemical analyses demonstrated that $CoSe_2$@RGO composites have excellent catalytic activity for reduction of I_3^-, exhibiting synergetic effect between $CoSe_2$ and RGO. As a consequence, the DSSC using the $CoSe_2$@RGO CE showed the comparable power conversion efficiency (7.01 %) to the Pt-based CE device (6.77 %). Therefore, the composites of $CoSe_2$ with RGO can be good candidates as catalyst materials instead of Pt.

Contents

List of Figures

List of Tables

Chapter 1. Introduction of Solar Cells

1. Energy crisis and renewable energy sources

The fossil fuels such as coal, petroleum and natural gas have become the best energy source in the 20th century, because they are inexpensive and yield higher energy than any other energy sources. Thus, the fossil fuels have been widely used to transportations, heating, power generation and etc., which account for 85% of all energy resources. However, they also have critical issues; first, the limitation of reserves. Though reserve/production ratio of coal, petroleum and natural gas is different, it is obvious that those fuels are not infinite resources. If alternatives are not secured until fossil fuels are totally exhausted, we will be suffering from lack of energy. Another problem is the air pollution. The sulfur oxides (SO_x), nitrogen oxides (NO_x), carbon monoxide (CO) and etc. which come from combustion of fossil fuels lead to severe pollution problems. The efforts to prevent this issue have been concentrated such as the Kyoto protocol in 2005, but air pollution that comes from the fossil fuels not easily decrease with increasing the number of the world population. Although nuclear power plants, which is clearer and more efficient energy than the fossil fuels, are also operating, disbelief of nuclear power is constantly growing due to accidents of radioactive effluent such as nuclear disasters at Chernobyl in 1986 and at Fukushima in 2011.

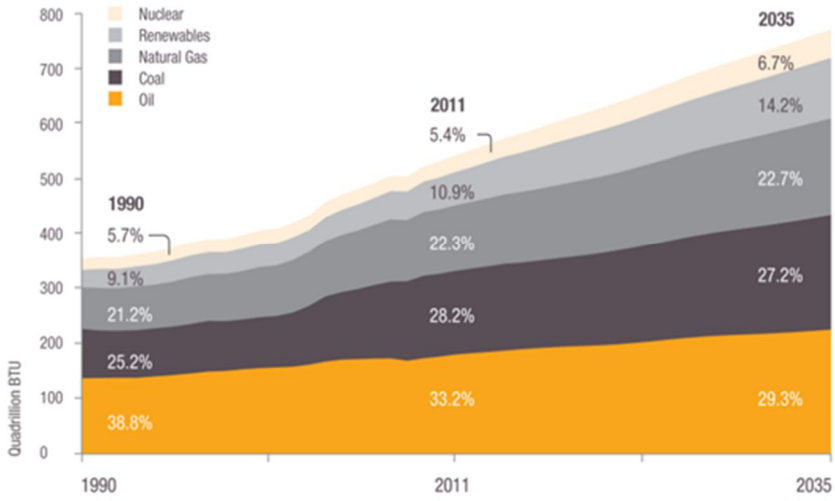

<Figure 1> The history and predict of global energy demand from 1990 to 2035.

Recently, renewable energy has been spotlighted because of these energy problems. Renewable energy means the energy that utilize eco-friendly resources such as sunlight, wind, geothermy, tidal power and etc. Unlike the fossil fuels, it is not needed to consider the exhaustion of energy sources because those sources are unlimitedly supplied to us as the earth and the sun exist. Furthermore, the hazardness of renewable energy sources and the pollution emissions from renewable energy generating process are extremely low compared to the fossil fuels. Also, there is no leakage danger of radioactive materials like the nuclear power. For these reasons, the use of the renewable energy is gradually increasing. As indicated in figure 1, the percentage of the energy consumption of the renewable energy in 1990 was 9.1% but in 2011 increased to 10.9%. Nowadays, the researches for the improvement of energy conversion efficiency and enhancement the market competitiveness are being concentrated, and the use of the renewable energy is expected to further increase to 14.2% by 2035.

<Figure 2> Average annual growth rates of renewable energy capacity from end-2008 to 2013. CSP means concentrating solar thermal power.[1]

Especially, the growth of solar photovoltaics (PV) are remarkable. PV are a kind of devices which generate electrical power by converting sunlight into electric current. It shows higher energy conversion efficiency than other renewable energy sources, and the positioning of its module systems is less influenced by environments compared to others. Thanks to these advantages, PV are already commercialized and world-widely utilized. Moreover, PV are still growing rapidly showing the highest growth rate of the average annual growth rates of the renewable energy capacity in 2013.

2. Types of solar cells

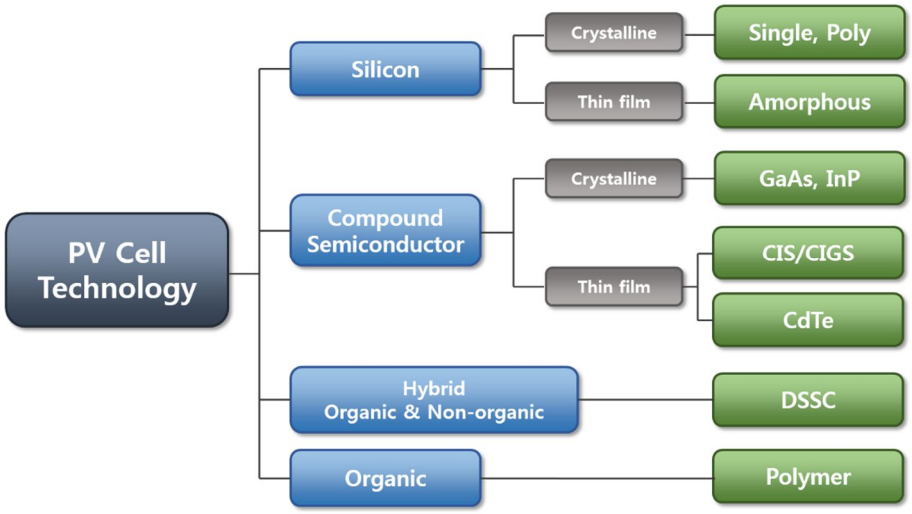

<Figure 3> Types of solar cells categorized according to materials.

Figure 3 shows various types of solar cells. The first generation of solar cells is the silicon solar cell, which is the first commercialized solar cell in 1954. The Si-based solar cell is fabricated by combining n-type silicon and p-type silicon forming PN junction and depletion layer, and generate current by the photovoltaic effect when sunlight irradiates the semiconductor layer. Among all kinds of solar cells, single crystalline Si (sc-Si) solar cells have been widely used because of high photon-to-current efficiency. However, the cost is very expensive in terms of both Si semiconductors with good crystallinity and the manufacture process. For this reason, polycrystalline- (pc-) and amorphous Si solar cells which are cheaper than sc-Si have been developed. But those Si solar cells exhibited lower efficiency and shorter life time than the sc-Si based solar cells.

Meanwhile, the efforts have been concentrated to fabricate solar cells using the compounds of metals and/or semiconductors except for Si. One example is gallium arsenide (GaAs) solar cells. The advantages of GaAs are higher efficiency than sc-Si solar cells due to outstanding electron mobility and 1.43 eV of direct band gap. But the GaAs material is more expensive and heavier than sc-Si. Another examples are copper indium gallium diselenide (CIGS) and cadmium telluride (CdTe) solar cells also called as the second generation solar cells or thin film solar cells. These solar cells do not need expensive manufacture process as sc-Si solar cells and can be fabricated on flexible substrates due to their thin thickness. Therefore, they can be applied to textile products or foldable devices. Though second generation solar cells have many advantages, some drawbacks still hinder commercialization of them due to low efficiency, and in case of CdTe, toxicity of cadmium.

Nowadays, the third generation solar cells are being spotlighted. These state-of-the-art solar cells include organic polymer solar cells and dye-sensitized solar cells (DSSCs). One of the features of polymer solar cells or organic photovoltaics (OPVs) is the use of a polymer. It means that it is possible to tune properties such as the energy gap by changing the sorts or functional groups of polymers. Furthermore, OPVs are thin and solution-processible, so that it facilitates roll-to-roll process. DSSCs are also very promising next-generation solar cells. The working principle of DSSCs is similar with the photosynthesis of plants. In other words, DSSCs operate through not the PN junction but an electrochemical reaction unlike the other solar cells. DSSCs can be fabricated by facile methods in laboratories as well as even home and the cost materials used are low-cost. Although both OPVs and DSSCs do not show low efficiency and low stability yet, they have large potential to be applied to various devices such as flexible electronics with chip price.

Chapter 2. Dye-sensitized Solar Cell

1. Introduction

Dye-sensitized solar cells (DSSCs) are devices that generate electrical energy from light-sensitized dyes. As chlorophyll in plants receives sunlight and plants produce oxygen through photosynthesis, excited electrons in dye materials produced by sunlight generate current. Unlike silicon-based solar cells, electrons in DSSCs are transported by electrochemical methods. So DSSCs are also called as electrochemical devices.

The history of DSSCs have begun in 1972 by Memming.[2] At that time, it was confirmed that electrons from light-sensitized dye can move into semiconductors anchored with dye molecules. After 5 years, in 1977, Matsumura et al. observed photovoltaic properties by using zinc oxide semiconductors and natural dyes such as Rose Bengal in 'Wet-type' photocells.[3] However, conversion efficiency was too poor recording only 1.5% at specific wavelength. In 1991, O'Regan and Grätzel's research results innovatively developed DSSCs.[4] They fabricated photon-to-current conversion devices like a sandwich shape by bonding working electrodes and counter electrodes. As the result, 7.12% of power conversion efficiency was obtained at simulated 1 SUN light. After this study, the boom of DSSCs occurred. Many researchers dived into DSSC studies. Due to these efforts, the field of DSSCs was further developed. Now 2014, the officially recorded world-best efficiency of DSSCs is 11.9%. It was obtained by Sharp Company in Japan with 1 cm^2 area cells.

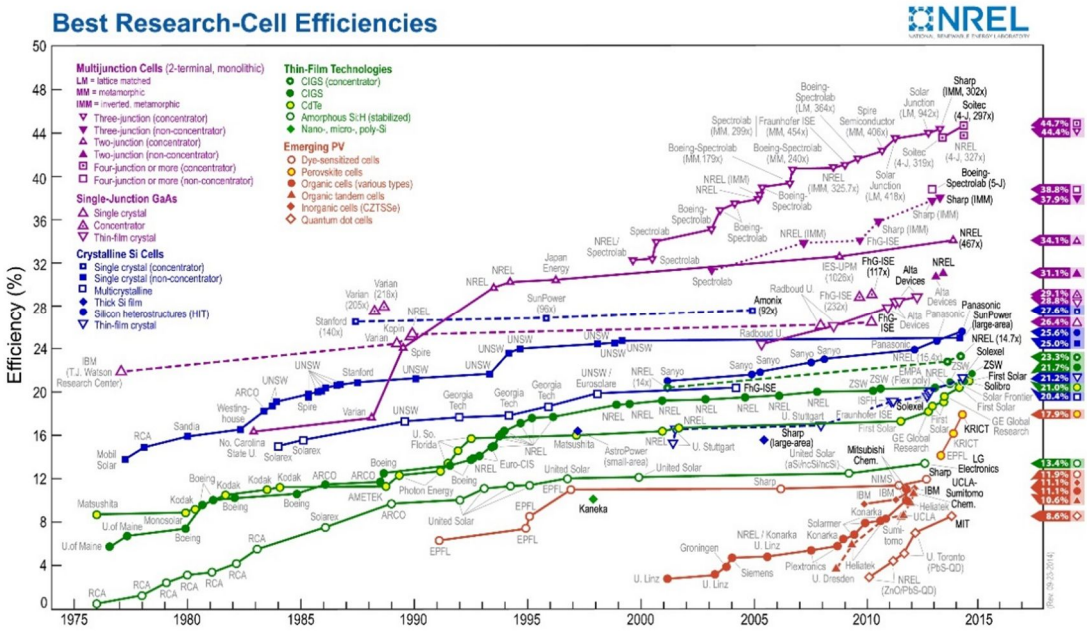

<Figure 4> The efficiency chart of various photovoltaics (Source: NREL, 2014)

DSSCs have been regarded as one of the most promising next-generation solar cells because they have many advantages such as low-cost, easy fabrication and lightness. Since Grätzel's group developed DSSCs using nanocrystalline titanium dioxide (TiO_2), metal complex dyes, redox couple electrolytes and platinized fluorine-doped tin oxide (FTO), these materials have become base materials of DSSCs.

2. Structure of dye-sensitized solar cells

2. 1. Working principle of dye-sensitized solar cell

Dye-sensitized solar cells (DSSCs) are photovoltaics which absorb light corresponding to wavelength of visible-light area to near-infrared, then generate electricity. Usually, the device is composed of the transparent conductive oxide (TCO) glass, the nanocrytailline metal oxide semiconductors, the dye molecules as light-sensitizer, redox couple electrolytes and platinized on TCO substrates. An overall structure of the DSSC is shown in Figure 5. On the glass coated with TCO such as fluorine-doped tin oxide (FTO), metal oxide, generally nanocrystalline titanium dioxide (nc-TiO_2) layers comprised of optically transparent, 20 nm-sized nanoparticles are deposited with approximately 10 ~ 12 μm thickness. Transition metal complex dye molecules like N719 ruthenium complex are adsorbed on surfaces of nc-TiO_2. The set of TCO glass substrates, nc-TiO_2 coated with dye molecules are called as a working electrode. An opposite electrode is the counter electrode. The structure of counter electrode is simpler than working electrode. Extremely thin platinum layers are formed on the TCO glass. These two electrodes are bonded with Surlyn resin spacer, making a few tens μm distance. Between two electrodes, the iodide/triiodide (I^-/I_3^-) redox couple liquid electrolyte are fully filled in pores of nc-TiO_2 layers.

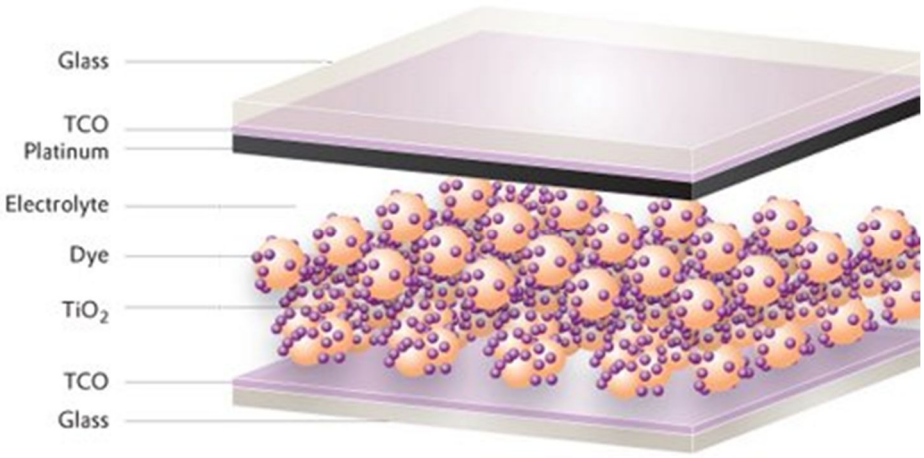

<Figure 5> A schematic of the typical structure of a dye-sensitized solar cell

DSSCs can be operated as photovoltaics upon being irradiated by sunlight. When dye-sensitizers absorb light which has enough photon energy to excite electrons in dye molecules, they become an

excited state (S*) from a ground state (S). Then, electrons in the dye molecules are quickly injected to the conduction band (CB) of nc-TiO_2 in fs ~ ps time scale, leaving the dye molecules to an oxidized state (S^+). The injected electrons percolate through the porous nc-TiO_2 particles to the FTO of the glass substrate. The above-mentioned process occurs in the working electrode (WE), i.e., anode of a DSSC. After that, electrons flow along with the external circuit connected with the anode and reach to the cathode, in other words, counter electrode (CE). Due to presence of platinum catalysts at CE, triiodide ion (I_3^-) species in the redox couple liquid electrolyte are easily reduced to iodide ion (I^-) at the surface of the CE. When I^- species are diffused to the oxidized dye molecules, dye molecules are reduced from the oxidized state (S^+) to the ground state (S). This series of the cycle between the WE and the CE is circulated as long as light exist. Figure 6 shows the process and summarization of the operating cycle in terms of chemical reaction is indicated in Equation 2.1.

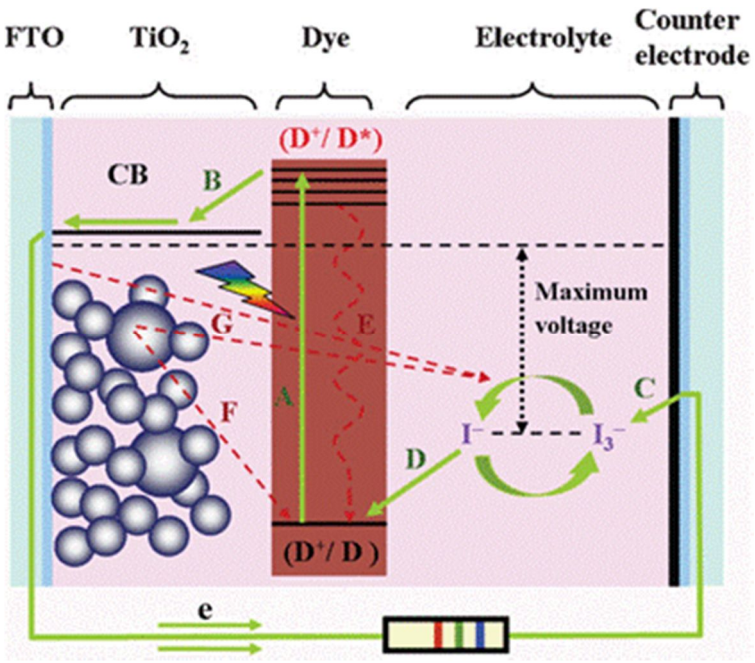

<Figure 6> A diagram showing the energy level and the electron transfer process of a dye-sensitized solar cell

$S + h\nu \rightarrow S^*$	*Excitation process*	
$S^* \rightarrow S^+ + e^-_{(TiO2)}$	*Electron injection*	
$e^-_{(TiO2)} \rightarrow e^-_{(Pt)}$ + energy	*Energy generation*	
$I_3^- + 2e^-_{(Pt)} \rightarrow 3I^-$	*Electron capture reaction*	
$2S^+ + 3I^- \rightarrow 2S + I_3^-$	*Regeneration of dye*	(2.1)

The theoretical maximum voltage, i.e., open-circuit voltage of DSSCs is determined by the difference between the quasi-Fermi level of the TiO_2 and the redox potential of I^-/I_3^- couple. Thus, the voltage can be decreased when the quasi-Fermi level of the TiO_2 gets lowered. The cause of quasi-Fermi level decrease is recombination at various sites, for example, the relaxation of electrons in the excited state of lowest-unoccupied molecular orbital (LUMO) of the dye, the recombination from the CB of the TiO_2 or FTO to the highest-occupied molecular orbital (HOMO) of the oxidized dye, and participation of unnecessary electrons to I^-/I_3^- redox couple reaction.

2. 2. Transparent conductive oxide

Typically, DSSCs are fabricated on the glass coated with transparent conductive oxide (TCO) materials. TCO allow electrons to move on the substrate and light to irradiate the working electrode of the device so that dye molecules absorb it. Therefore, not only high conductivity but also high transparency are important factors for TCO. The material which can simultaneously satisfy these properties is indium tin oxide (ITO). ITO is widely utilized for electronic and mechanical industries already due to their superior transmittance and conductivity, corresponding to ~95% and 10^4 W^{-1} cm^{-1}, respectively.[5] However, in DSSCs, fluorine-doped tin oxide (FTO) is mainly used rather than ITO, even transparency of FTO is inferior to ITO. The critical reason is thermal stability. In the general process of the DSSC fabrication, High temperature exceeding 450 °C is required in an oxygen atmosphere. While sheet resistance of FTO remained constant after sintering, that of ITO increased about four-fold.[6] Therefore, FTO is recommended for the TCO substrates.

Some researches shows the DSSCs successfully fabricated using TCO-free substrates. Flexible TiO_2 metal mesh substrate made through titanium sputtering was applied for a photoanode[7], conductive polymers such as poly(3,4-ethylenedioxythiophene) (PEDOT) was used for a counter electrode.[8] Though these DSSCs did not exhibit higher efficiency than commercial DSSCs, they suggest that TCO-free substrates can be utilized usefully because expensive TCO materials can be substituted.

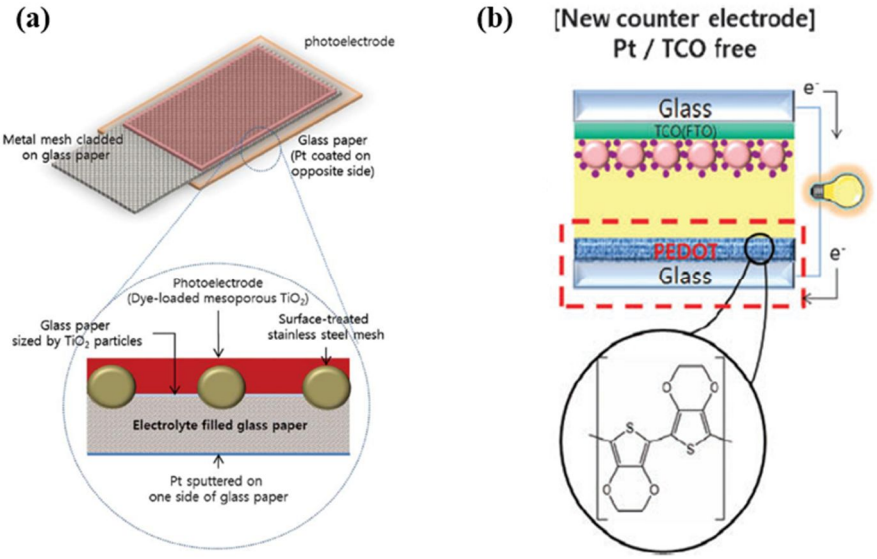

<Figure 7> Dye-sensitized solar cells by using TCO-free substrates. (a) The TiO_2-coated metal mesh substrate for a working electrode, (b) The PEDOT glass substrate for a counter electrode. Reproduced in part with permission from ref. 7 and 8.

2. 3. Nanostructured semiconductor of working electrode

Before Grätzel group's study about dye-sensitized solar cells (DSSCs), power conversion efficiency of devices was very poor, less than 1%. However, after Grätzel's research, efficiency dramatically rose exceeding 7%. The reason why his research could be the breakthrough is the usage of nanocrystalline TiO_2 (nc-TiO_2). In previous studies, a semiconductor material for the working electrode (WE) was smooth-surfaced bulk TiO_2. Planar-structured semiconductors made the dye molecules be adsorbed onto only the top layer of the TiO_2 film. Thus, it could not be able to yield high current using the WE to which a not sufficient amount of the dye was adsorbed. On the other hand, in Grätzel group's DSSCs, nc-TiO_2 composed of 20 nm nanoparticles made a tremendous number of pores and drastically widened the surface area of TiO_2. As the result, a larger amount of dye molecules could be adsorbed, so that more current generated resulting in increment of efficiency.

Therefore, the large surface area of semiconductors and the loading amount of dye molecules are important for efficient DSSCs. Besides, not only above two factors but also following factors are significant; band gap, stability. The band gap of the semiconductor should be large enough to penetrate the light which has longer wavelength than ultraviolet (UV), i.e., to allow dyes to absorb visible-light. Also, it is recommended that the conduction band (CB) of semiconductors matches with the CB of the dye. If the CB of semiconductors is bigger than the CB of dyes, electrons from the dye of excited states cannot be transferred to semiconductors. If too much smaller, open-circuit potential (V_{oc}) of DSSCs decreases. Because of the usage of dye solution using organic solvent for the dye adsorption process and liquid electrolyte based on iodide/triiodide (I^-/I_3^-) couple, stability against these chemicals is needed.

The semiconductor material which can fulfill these all requirements is TiO_2. TiO_2 has wide band gap (~ 3.2 eV), and the CB (-4.2 eV) is well matched with the LUMO of dyes such as N719 (-3.9 eV), N749 (-3.8 eV)[9] and N3 (-3.8 eV)[10], etc. TiO_2 also shows outstanding chemical stability in iodide liquid electrolytes. Furthermore, it is earth abundant, non-toxic and has 90% of high optical transmittance about visible-light.

There are three kinds of TiO_2 crystalline structures; anatase, rutile and brookite (see Figure 8). Among these, anatase and rutile are considered as semiconducting materials for the WE of DSSCs. While each unit cell of rutile TiO_2 is connected by its edge, anatase is by its side. Moreover, the Ti-Ti distance of anatase (3.79 Å, 3.04 Å) is longer than rutile (3.57 Å, 2.96 Å) and vice versa in case of the Ti-O distance (anatase: 1.93 Å, 1.98 Å; rutile: 1.95 Å, 1.98 Å). Because of these differences, they exhibit different electrical properties and porosity. Park et al. reported that anatase TiO_2 can adsorb a more amount of dye molecules than rutile, because crystal shape of anatase is a sphere whereas rutile is a rectangular so surface area per unit volume of anatase is larger than rutile. Also, electron transport is faster in anatase than in rutile due to differences of interparticle connectivity associated with the

particle packing density.[11]

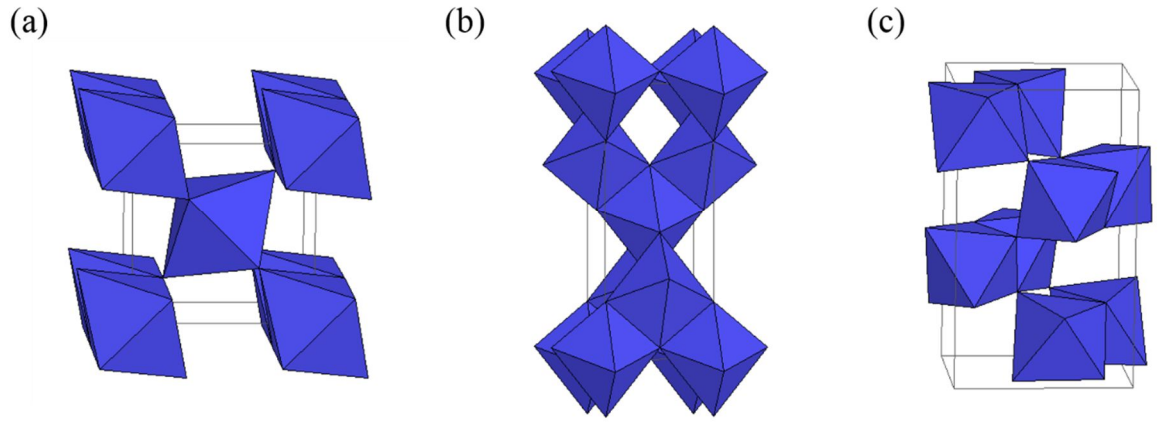

<Figure 8> The different kinds of TiO_2 crystal structures corresponding to (a) tetragonal rutile, (b) tetragonal anatase and (c) orthorhombic brookite.

Although TiO_2 is the most widely utilized semiconductor for DSSCs, zinc oxide (ZnO) is also a promising candidate. The band gap (3.0 ~ 3.2 eV) and conduction band edge of ZnO are similar to that of anatase TiO_2, but electron mobility of ZnO (205 ~ 300 cm^2 V s^{-1}) is 2 orders of magnitude higher than that of TiO_2 (0.1 ~ 4 cm^2 V s^{-1}). This higher electron mobility is expected to enhance electron transport. However, the power conversion efficiency of DSSCs using ZnO (7.5%) is significantly lower than that of TiO_2 (12.3%). The limited performance in ZnO-based DSSCs may be explained by the instability of ZnO in acidic dye (i.e., protons from the dyes cause the dissolution of Zn atoms at ZnO surface, resulting in the formation of excessive Zn^{2+}/dye agglomerates) and the slow electron-injection kinetics from dye to ZnO.[12]

The large efforts have been paid to change the nanostructure of the semiconductors. In commercial DSSCs, around 20 nm size nanoparticles of the semiconductors are used. It can give dye molecules a lot of sites to be anchored to the surface of semiconductors, but makes a large number of interfaces between particles which interrupt electron transport. For this reason, nanowire[13,14], nanorod[15], nanotube[16-18] and other nanostructures[19,20] have been studied. These studies are motivated by the expectation of an improved and directed charge transport along the nanostructures. Recombination rate could decline and charge collection could be improved by using these nanostructures. Nevertheless, photovoltaic performances were still lower than nanoparticle-structured devices because the internal surface area of those nanostructures was quite small compared to the nanoparticles.

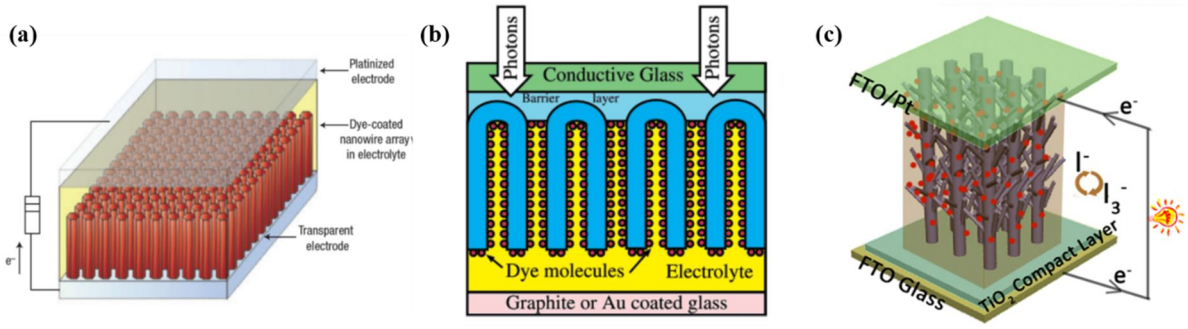

<Figure 9> (a) Nanowire, (b) nanotube and (c) nanobranch semiconductors for the working electrode of the dye-sensitized solar cell. Reproduced in part with permission from ref. 14, 16 and 20.

2. 4. Light sensitizer

The most crucial part of dye-sensitized solar cells (DSSCs) is the light sensitizer because charge carriers to operate the devices are produced from it. This should fulfill some essential characteristics: (i) The adsorption spectrum should be wide enough to cover the whole region of visible-light. It would be better to adsorb even the part of near-infrared (NIR) region. (ii) The light sensitizer should have anchoring groups such as –COOH, $–H_2PO_3$, $–SO_3H$ and etc. to strongly bind the dye onto the semiconductor surface. (iii) The lowest unoccupied molecular level (LUMO) of the light sensitizer should be higher than the conduction band (CB) edge of n-type semiconductors (TiO_2, ZnO, etc.), so that efficient electron transfer process between the excited dye and CB of the semiconductor can take place. (iv) For dye regeneration, the oxidized state level of the light sensitizer must be lower than the redox potential of electrolyte. (v) The light sensitizer should be stable to light, and electrochemical and thermal stability are also required. Based on these requirements, many kinds of dye sensitizers including metal complexes and metal-free organic dyes have been designed and applied to DSSCs.

Ruthenium (Ru) complexes are most widely used for the light sensitizer because of their broad absorption spectrum, suitable excited state energy level, relatively long excited-state life time and good electrochemical stability. Representatively, cis-$(SCN)_2$bis(2,2′-bipyridyl-4,4′-dicarboxylate)rutheni-um(II) (N3), Ru(4,4′,4″-tricarboxy-2,2′:6′,2″-terpyridine)$(NCS)_3$ (N749, black dye), and $(Bu_4N)_2[Ru(dcbpyH)_2(NCS)_2]$ (N719) are promising Ru complexes. Especially, the N719, which was investigated by Nazeeruddin et. al.[21], exhibited improved power conversion efficiency (>11%) under AM 1.5G irradiation.

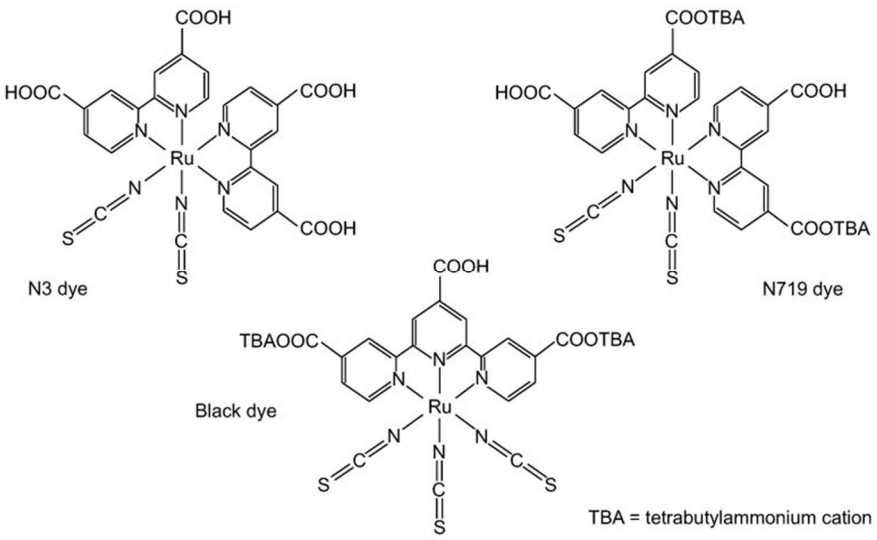

<Figure 10> Molecular structures of the N3, the black dye (N749) and the N719

However, these Ru complex-based dye cannot absorb the NIR region, i.e., it cannot fully generate more electrons from photons in sunlight. Porphyrin and phthalocyanine, the metal-free organic dyes exhibit panchromatic absorption spectrum with good chemical, photo-, and thermal stability. Nevertheless, the efficiency of DSSCs using the organic dyes were still lower than the Ru-based dyes due to significantly reduced lifetime[22] and the fast recombination in case of porphyrin-, phthalocyanine-based DSSCs, respectively.

Except for the dyes, other kinds of the light sensitizer have been extensively developed, including bandgap-tunable quantum dots (CdSe[23], PbS[24], etc.), Sb_2S_3[25], organic-inorganic hybrid lead halide[26], and etc.

2. 5. Electrolyte

In dye-sensitized solar cells (DSSCs), an iodide/triiodide (I^-/I_3^-) redox couple whose redox potential is more positive than the highest orbital molecular orbital (HOMO) of the dye is usually employed as an efficient electron mediator in an electrolyte. The function of the redox couple is to reduce the oxidized dye following electron injection from the counter electrode (CE), in other words, carry the charge back and forth between the working electrode (WE) and the CE.

The redox couple is generally used after dissolved in the organic solvents. The selection of the electrolyte solvent is important because it influences the photovoltaic performances such as open-circuit voltage (V_{oc}) and short-circuit current density (J_{sc}). Polar aprotic solvents such as acetonitrile are preferred as they offer good electrochemical stability, and solubility for redox mediators. Meanwhile, it is difficult to obtain high efficiency by using redox couple itself. Proper additives are necessary in the electrolytes. It has been found that the device performance can improve with nitrogen-containing heterocyclic compounds such as 4-*tert*-butylpyridine (tBP).[27] The effect of employing tBP is the improved V_{oc}. It is because of the suppression of the back electron transfer at the dyed-TiO_2/electrolyte junction. The pyridine molecules were expected to adsorb onto the TiO_2 surface, thus preventing the invasion of I_3^- and decreasing the rate of undesirable electron transfer from the TiO_2 to I_3^-. Cations such as Li^+ from lithium iodide (LiI), as counter ions of I^- and I_3^- in the electrolytes, play an important role in DSSCs.[28] They can efficiently protect photo-injected electrons on the TiO_2 film. Guanidinium thiocyanate (GSCN) has been found to inhibit the recombination rate by a factor of 20, which causes an increase of V_{oc}. Another redox couple species were also developed, because I^-/I_3^- redox mediator has some disadvantages: low redox potential which limits the V_{oc}, and its corrosivity on most metals. A cobalt (II/III) complex, $[Co^{II/III}(dbbip)_2](ClO_4)_2$ (dbbip: 2,6-bis(1-butylbenzimidazol-2-yl)pyridine) is the powerful candidate to substitute the iodide redox mediator. An advantage of these species is higher redox potential than the iodide. Although they do not match the N719 dye very well, 12.3% of power conversion efficiency, which is the best record of DSSCs in the laboratory scale, was achieved by Grätzel's group using cobalt redox mediators with porphyrin dyes.[29]

However, volatile liquid-based electrolytes have the evaporation or leakage problem. It deteriorates the stability of devices and hinders the possibility of commercialization. To overcome this shortage, quasi- or solid-state electrolytes have been studied. Quasi-solid state electrolytes can be realized by using ionic liquid[30] or mixing the liquid electrolytes with polymers[31] or organic gelators[32]. In case of solid electroytes, hole conducting materials such as 2,2',7,7'-Tetrakis-(N,N-di-4-methoxyphenylamino)-9,9'-spirobifluorene (Spiro-OMeTAD) were introduced.[33] Due to low volatility of these electrolytes, the leakage problem was resolved, but the ionic conductivity sharply decreased that resulted in the lower efficiency than liquid electrolytes.

2. 6. Materials of counter electrode

The electron transfer cycle of dye-sensitized solar cells (DSSCs) cannot be realized without catalysts on a counter electrode (CE), i.e., the catalysts play important roles in terms of the operation of the devices. In the presence of the catalysts, the oxidized species triiodide (I_3^-) of the electrolyte accept electrons from the CE then reduced to the iodide (I^-) which transfer electrons to oxidized dye molecules. Platinum is the most widely used material for the catalyst of DSSCs because of their excellent electrocatalytic ability and chemical stability. Pt can be deposited on transparent conductive oxide (TCO) substrates by using various methods such as electrodeposition, spray pyrolysis, sputtering and thermal decomposition. Among these, the thermal decomposition showed good performance and long-term stability.[34] This method is conducted by drop-casting or spin-coating method of hydrogen hexachloroplatinate(IV) hydrate ($H_2PtCl_6 \cdot xH_2O$) solution in ethanol or 2-propanol followed by heat treatment above 400 °C.

Though Pt is the most suitable material of the catalysts for triiodide reduction reaction, the problems to have to be solved still remain. Pt is a rare metal, so it hinders the large-area fabrication of DSSCs. Therefore, the Pt catalyst is highly recommended to be replaced to cheaper materials. As such efforts, alternative catalysts such as carbon materials and conducting polymers have been researched. Carbon materials such as carbon nanotubes (CNTs)[35], ordered mesoporous carbons (OMCs)[36] and graphene[37] can be practical materials because of abundance and good electronic conductivity. Also, they showed good catalytic properties for triiodide reduction with very high surface area. In case of conducting polymers, poly(3,4-ethylenedioxythiphene) was applied to the CE.[8] PEDOT also showed good catalytic properties and low charge transfer resistance below 1 Ω cm^2, which is similar with that of Pt. The CE using PEDOT not require high temperature as platinized CE, so it can be applied for the DSSCs which have to be fabricated under low temperature (<150 °C), for example, the DSSCs based on polyethylene naphthalate (PEN) substrates. Despite application of these catalyst materials, the electrocatalytic performances of both carbon and polymers are still lower than Pt. To overcome this shortage, combined materials such as CNTs/graphene, Pt/graphene and polymer/graphene were also developed.

Recently, metal chalcogenides (MCs) have emerged as realistically alternative materials for the CE. Some researches demonstrated that the DSSCs using several kinds of MCs (cobalt sulfide[38], iron sulfide[39] and etc.) show efficient electrocatalytic effects in the I^-/I_3^- electrolyte with remarkable stability, and yield higher power conversion efficiency than carbon- or polymer-based CEs, even Pt-based CEs.

E substrate	Catalyst on CE	Electrolyte solvent	Cell area (cm^2)	Light intensity ($mW\ cm^{-2}$)	J_{sc} ($mA\ cm^{-2}$)	V_{oc} (mV)	FF (%)	η (%)	Authors	Year
	Graphite and carbon black	Acetonitrile	0.4	100	11.34	826	71	6.67	Kay and Grätzel	1996
FTO-glass	Carbon black	Polypyrrole (solid state)		10	0.104	716	78	0.62	Kitamura et al.	2001
ITO-glass	PEDOT-TsO	3-Methoxyacetonitrile	0.35	100	11.2	670	61	4.60	Saito et al.	2002
Glass	Single wall carbon nanotubes	3-Methoxyacetonitrile	0.25	100	9.7[a]	750[a]	62[a]	4.5	Suzuki et al.	2003
FTO-glass	Activated carbon	Acetonitrile	0.05	100	7.93	808	61	3.89	Imoto et al.	2003
Au	PEDOT	– (solid state)		100	2.6	680	51	0.93	Fukuri et al.	2004
Stainless steel	Pt	3-Methoxypropionitrile	0.2	100	12.4	703	60	5.24	Ma et al.	2004
Au/FTO-glass	PEDOT	Poly(3-thiophenylacetic acid) (solid state)		100	2.5	365	54	0.5	Senadeera et al.	2005
FTO-glass	Carbon black	Acetonitrile + Valeronitrile	0.16	100	16.8	790	69	9.1	Murakami et al.	2006
FTO-glass	Carbon black and polyaniline	1,3-diethyleneoxideimidazolium iodide (semisolid state)	0.24	100	12.8	580	47	3.48	Ikeda et al.	2006
ITO-glass	Polyvinyl pyrrolidone-capped platinum	3-Methoxypropionitrile	0.25	100	10.5	660	41	2.84	Wei et al.	2006
ITO-PEN	Pt	Acetonitrile + Valeronitrile		100	13.6	780	68	7.2	Ito et al.	2006
FTO-glass	Pt	Acetonitrile + Valeronitrile	0.16	100	17.73	846	75	11.18	Nazeeruddin et al.	2006
Stainless steel	Carbon black	Acetonitrile + Valeronitrile	0.16	100	16.3	785	71.	9.15	Murakami et al.	2007

<Table 1> Typical performances of the dye-sensitized solar cells with different types of counter electrodes. Reprinted in part with permission from ref. 40

3. Prospects of dye-sensitized solar cells

Dye-sensitized solar cells (DSSCs), which are one of the next-generation solar cells, have been given attentions because of their advantages such as low-cost and easy fabrication. Since the development of DSSCs in 1991 by Grätzel's group DSSCs have been steadily improved for a few decades, and now, the commercialization of DSSCs are also being studied.

One of these efforts is flexible DSSCs. DSSCs can be easily destroyed or broke down by physical impacts because DSSCs are usually fabricated by using rigid glass substrates. But it can be free from these problems if flexible plastic-substrates such as indium tin oxide (ITO) coated polyethylene naphthalate (PEN) or polyethylene terephthalate (PET) are employed to DSSCs. Moreover, the devices can be fabricated thinner and lighter than glass-based devices by using flexible substrates, and widely utilized to various sources due to their 'flexible' properties. For example, it is possible to combine with portable electronics such as lap-tops, cell phones and watches, and apply to wearable devices. However, a severe problem of plastic substrates is to form mesoporous metal oxide layers. Generally, the calcination of titanium oxide (TiO_2) or zinc oxide (ZnO) at approximately 500 °C is required to be strongly adsorbed onto the substrates and induce their electronic conductivity. Both PEN and PET cannot endure the heat above 150 °C thus the flexible DSSCs using plastic substrates have to be fabricated low temperature. As the solutions, electrochemical deposition, lift technique and other methods were conducted and the metal substrates such as steel use stainless (SUS) were introduced.[41]

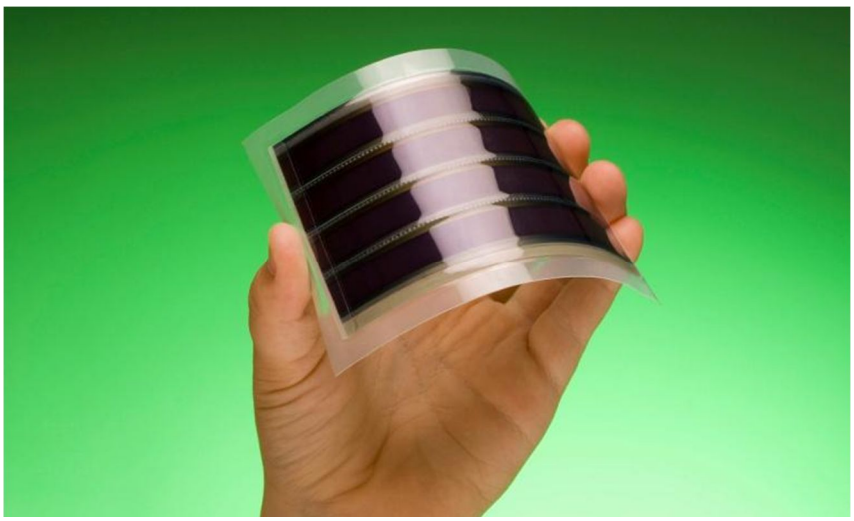

<Figure 11> A flexible dye-sensitized solar cell based on an ITO-PEN substrate.

Fiber-type DSSCs are also being researched. Unlike the planar-shape sandwich type DSSCs, the fiber DSSCs, which is based on the TiO_2 photoanode from anodized titanium metal wire, have an advantage; no limitation on incidence angle of light. Although the power conversion efficiency of the fiber DSSCs is significantly lower than planar DSSCs, it is worthwhile to develop further because it can be utilized as a textile and a wearable device in the near future.

Meanwhile, DSSCs can be fabricated with various colors depending on the dyes, generate electricity even in weak sunlight and have a little bit transparency compared to silicon solar cells. Through these advantages, DSSCs can be applied to building integrated photovoltaic system (BIPV). When DSSCs are used in windows, energy loss come from windows can be reduced and it can provide visual pleasures through diverse colors and designs.

<Figure 12> Examples on applications of DSSCs. the colorful and splendidly designed DSSC (left) and the BIPV using DSSC panels (right, reprinted with permission from DYESOL, Australia).

Though it is worthwhile to commercialize DSSCs owing to their many advantages, some problems to be resolved still remain. A representative example is the leakage of the electrolyte. The liquid-phase electrolytes are commercially used for DSSCs to enhance electron conductivity. However, the liquid can escape through the gap between a working electrode and a counter electrode of the device. It is strongly related with long-term stability of the devices and the obstacle about commercialization of DSSCs. Another problem is lower conversion efficiency than silicon based solar cells. The silicon solar modules (multicrystalline) yield 19.5% of conversion efficiency in 242.7 cm^2 area, while that of the dye-sensitized solar modules is around 10% even in smaller area, 17.11 cm^2.[42] The production cost of DSSCs is cheaper than that of silicon solar cells. Nonetheless, efficiency of DSSCs should be further improved to succeed in commercialization. If it is possible to overcome these shortages, the market of DSSCs will grow rapidly as the innovative renewable energy.

Chapter 3. Synthesis of $CoSe_2$@RGO and Its Application in Dye-sensitized Solar Cells

1. Introduction

A typical DSSC is comprised of a dye-coated nanocrystalline titanium oxide (TiO_2), I^-/I_3^- redox mediator and a platinum- (Pt) coated counter electrode (CE). Extensive researches have been conducted in order that each component achieves highly efficient DSSCs, including materials for the CE. Pt is the most widely used material as the catalyst of DSSCs due to its superior electrocatalytic properties and chemical stability. However, highly expensive rare metal Pt interrupts the production of large-area DSSCs. Moreover, stable Pt finally corrodes in the iodide-based electrolyte forming PtI_4 or H_2PtI_6.[43] To construct the dye-sensitized solar module system, it is inevitable to develop alternative materials which must be inert and show good catalytic effect in the electrolyte simultaneously.

A lot of efforts have been taken to replace Pt with other cost-effective materials such as carbon derivatives [35-37]. Though carbon materials are low cost and show good chemical stability against I^-/I_3^- electrolyte, they do not exhibit catalytic activities as high as Pt yet. Recently, metal chalcogenide (MC) materials have emerged as a powerful candidate for the catalyst materials of the CE. The MCs have the formula MX_y, where M = a transition metal, X = chalcogen (S, Se and Te), and their physical and chemical properties vary according to the sort of M and X. Therefore, MCs are applied to a range of fields such as transistors and other energy conversion and storage devices.[44] Many kinds of MCs have been also applied to DSSCs as the catalyst materials for I_3^- reduction. Cobalt sulfide (CoS) was employed to the CE material of DSSCs as MCs for the first time by Wang, et al.[38] Deposited on a flexible substrate (ITO/PEN), it exhibited similar electrocatalytic effects with Pt and low charge transfer resistance corresponding to 1.8 Ω cm^2. After that, FeS_2[39], $Ni_{0.85}Se$[45], $NiSe_2$[46] and other MCs have been used to the CE of DSSCs and those CEs also showed superior performances with low charge transfer resistance. Besides, there is a report which demonstrates an improvement of power conversion efficiency of NiS_2 CE DSSCs when some amount of reduced graphene oxide (RGO) is combined with NiS_2.[47] It means that RGO distributes electrocatalytic properties of MC catalysts.

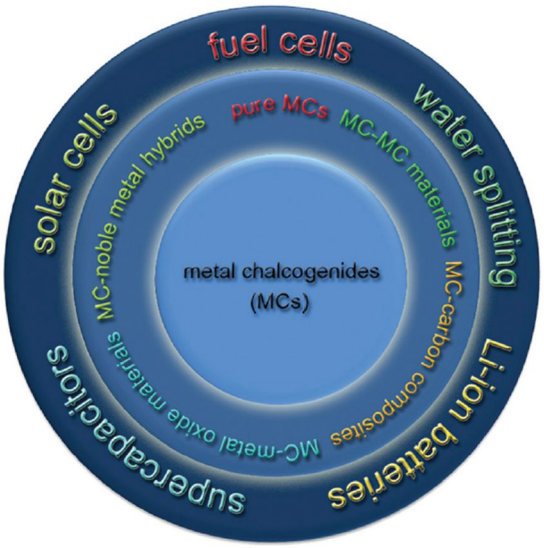

<Figure 13> Schematic illustration of metal chalcogenide (MC)/modified-MC materials and their potential applications in various ECS devices. Reprinted with permission from ref. 44

Meanwhile, cobalt diselenide ($CoSe_2$) supported by carbon derivatives has been studied as a prospective material for oxygen reduction reaction in polymer electrolyte membrane fuel cells (PEMFCs), exhibiting good catalytic effects and stability. However, there were no reports about application of the composites of $CoSe_2$ and graphene in DSSCs. Herein, I synthesized both $CoSe_2$ and mixed composites $CoSe_2$ with RGO ($CoSe_2$@RGO) by using one-step hydrothermal method. These composites were utilized to the CE of DSSCs for I_3^- reduction. Also, photovoltaic performances of those DSSCs were measured and their electrochemical properties were analyzed.

2. Experimental

Synthesis of $CoSe_2$, $CoSe_2$@RGO and RGO

$CoSe_2$ was synthesized via a facile hydrothermal reaction.[48] Selenium (Se) precursor solution (solution A) was prepared by dissolving 4 g of sodium hydroxide (NaOH, Aldrich, 99% anhydrous) in 30 ml of deionized water (DI water) followed by 0.32 g of selenium powder (Se, Aldrich, 99.999% metal basis) at a 80 °C hot plate overnight with stirring to dissolve Se completely. Cobalt (Co) precursor solution (solution B) was prepared by dissolving 0.31 g of ethyldiaminetetraacetic acid disodium salt dihydrate (EDTA-2Na, Sigma-Aldrich, 99.0-101.0%) in 10 ml of DI water with vigorous stirring for a few minutes followed by 0.48 g of cobalt chloride hexahydrate ($CoCl_2 \cdot 6H_2O$, Alfa Aesar, 99.9% metal basis). After heating solution B as same as temperature of solution A, solution B was slowly poured into solution A and the mixed solution was further stirred for 10 min on a heated hot plate. Then, the precursor solution was transferred to a Teflon-lined autoclave, and that was tightly sealed and heated at 170 °C for 12 h. After cooling down to room temperature naturally, the black precipitate was obtained and washed several times with water and ethanol. Finally, the product was dried in a vacuum oven at 60 °C for overnight.

In case of $CoSe_2$@RGO, the whole synthesis procedure is similar with $CoSe_2$ synthesis but solution C was added. 2.6 mg of graphene oxide (GO) sheets was uniformly dispersed by ultra-sonication in 8 ml of DI water to form solution C. Also, the amount of water in both solution A and B was adjusted to 25 ml and 7 ml, respectively.

To compare with the $CoSe_2$@RGO composites, pure RGO was also synthesized by using hydrothermal method. 30 mg of GO in 60 ml of DI water was treated in ultrasonic bath for 30 min and the dispersion was added to the autoclave directly. The hydrothermal reaction was conducted under same condition with the synthesis of cobalt diselenide derivatives. The precipitation was rinsed and washed several times then completely dried at 60 °C.

Preparation of TiO_2 working electrodes

Fluorine-doped tin oxide (FTO) glass substrate (TEC, 8 Ω, Pilkington) was cleaned with a detergent solution and then cleaned in an ultrasonic bath using ethanol, acetone and 2-propanol for 10 min, respectively. After O_2 plasma treatment for 10 min, The TiO_2 paste (ENB Korea, 20 nm) was coated on the substrate by using the doctor-blade method. The resulting layer was sintered at 500 °C for 2 h in a muffle furnace. The TiO_2-coated substrate was immersed in the N719 dye solution (0.3 mM in a mixture of *tert*-butanol and acetonitrile by a volume ratio of 1:1) for 24 h at room temperature.

Preparation of counter electrodes

$CoSe_2$ and $CoSe_2$@RGO suspension were prepared to deposit the catalysts onto the FTO glass. γ-Butyloractone (GBL) was selected as dispersion medium because of its good ability to disperse the synthesized compounds and slow evaporation rate. Therefore, $CoSe_2$ and $CoSe_2$@RGO powder were respectively dispersed in GBL with 0.7 mg/ml, 1.3 mg/ml and 2 mg/ml of concentration. Then, 200 μl of each dispersion was drop-casted onto O_2 plasma-cleaned 3 cm x 4 cm size FTO glass, so that the catalyst materials can be loaded onto the FTO glass with 10 μg/cm^2, 20 μg/cm^2 and 30 μg/cm^2. Those substrates were dried under ambient condition naturally for overnight and then heated at 200 °C for several minutes. For the comparison, RGO powder was also dispersed in GBL with 1.3 mg/ml of concentration. The rest of process was same with the preparation of $CoSe_2$ with/without RGO CE. In case of the platinized CE, 7 mM of chloroplatinic acid hexahydrate (H_2PtCl_6, Sigma-Aldrich) solution in 2-propanol (IPA) was prepared and 200 μl of that solution was drop-casted onto FTO substrate and sintered at 400 °C for 1 h. The final loading amount of Pt and RGO was fitted to 20 μg/cm^2.

Fabrication of DSSCs

Each 3 cm x 4 cm size anode and cathode was cut into 1.5 cm x 2.0 cm size pieces after finishing the process of immersion in dye solution or heat treatment. Two kinds of electrodes were combined by using hot-melt Surlyn (Solaronix, 60 μm) spacer. After that, iodide/triiodide redox shuttle electrolyte was injected through a pre-drilled hole and the holes were sealed by Surlyn and thin cover glass. The electrolyte composition was 1-hexyl-2,3-dimethyl-imidazolium iodide (0.6 M), iodine (0.03 M), guanidinium thiocyanate (0.1 M), and 4-*tert*-butylpyridine (0.5 M) in acetonitrile.

Characterization and measurement

The X-ray diffraction measurement was carried out with X-ray diffractometer (D8 Advance, Bruker) with Cu Kα radiation (λ = 0.154 nm). The morphology of $CoSe_2$ and $CoSe_2$@RGO was confirmed by field emission scanning electron microscope (FE-SEM, Hitachi S-4800 and Nova NanoSEM 230) and atomic ratio analysis of $CoSe_2$ was conducted by energy dispersive spectroscopy (EDS) connected with FE-SEM. The Raman spectra were obtained using micro-Raman spectrometer (Alpha 300R) with 633 nm laser. Surface chemical analyses were made by X-ray photoelectron spectroscopy (XPS, K-alpha, Thermo Fisher).

Electrochemical impedance spectroscopy (EIS) and Tafel polarization measurements were performed on the symmetrical dummy cells assembled with two identical electrodes filled with the same electrolyte as used in DSSCs. Scan range in EIS experiment was from 10^{-1} Hz to 10^6 Hz. In case of Tafel polarization, scan rate of voltage was 10 mV/s. Cyclic voltammetry (CV) was carried out in a

three-electrode system with a Pt-mesh as the CE and a saturated calomel electrode (Ag/Ag^+ electrode) as the reference electrode in electrolyte solution (0.1 M of $LiClO_4$, 0.01 M LiI, and 1 mM I_2 in acetonitrile). Scan rate in CV measurement was 50 mV/s. The current-voltage curves (*J-V* curves) of DSSCs with the different CEs were obtained using the current-voltage characteristic measurements under 100 mW/cm^2 AM 1.5G light (ABET Technology, LS 150 simulator) and photovoltaic parameters (short-circuit current density, open-circuit voltage, fil factor and power conversion efficiency) were characterized from the obtained *J-V* curves. All the electrochemical characterizations and photovoltaic measurements were performed by using an electrochemical station (Bio-Logic science instruments, VSP, CLB-2000).

3. Results

3.1. Characterization of as-synthesized materials

As-synthesized $CoSe_2$ and $CoSe_2$@RGO were analyzed using various instruments to identify the properties and structures. Figure 14 shows X-ray diffraction (XRD) patterns of graphene oxide (GO), reduced graphene oxide (RGO), $CoSe_2$ and $CoSe_2$@RGO, and Figure x shows the XRD peaks of as-synthesized $CoSe_2$ and $CoSe_2$@RGO, and the database peaks of orthorhombic $CoSe_2$. GO exhibited a XRD peak at 11.3°, corresponding to an interplanar spacing of 0.78 nm. After hydrothermal reaction of GO, the GO peak was disappeared and a broad peak of RGO newly appeared at 23.1°, corresponding to an interplanar spacing of 0.38 nm. The interplanar spacing of GO and RGO was calculated by using Bragg's equation, shown in Equation 3.1.

$$\mathrm{d} = \frac{\lambda}{2\sin\theta} \tag{3.1}$$

Where d is the interplanar spacing between the planes in the atomic lattice, λ is the wavelength of incident X-ray and θ is the angle between the incident ray and the scattering planes. As shown in Figure 15, all diffraction peaks of as-prepared $CoSe_2$ and $CoSe_2$@RGO samples were well matched to the standard XRD data of orthorhombic $CoSe_2$ (JCPDS no. 00-053-0449). Furthermore, the peaks of $CoSe_2$@RGO seems that the combination of RGO peaks and $CoSe_2$ peaks.

The morphology of $CoSe_2$ and $CoSe_2$@RGO was confirmed by field-emission scanning electron microscope (FE-SEM). The SEM images of the composites were shown in Figure 16. Synthesized $CoSe_2$ has sea urchin-like nanorod-based shape while in case of $CoSe_2$@RGO, some hexagonal-shaped sheets, which seem another kind of $CoSe_2$ crystals were mixed with $CoSe_2$ nanostructures. Energy-dispersive spectroscopy (EDS) analysis was conducted to confirm the exact stoichiometry of cobalt and selenium compounds. Figure 17 presents elemental analysis of the cobalt selenide composite and Figure 18 shows the distribution of Co and Se atoms. In addition, Table 2 indicates weight percentage and atomic percentage of the cobalt selenide composite. According to the EDS results, atomic percentage of cobalt and selenium was 30.15:69.85 which is close to the stoichiometric ratio of $CoSe_2$. Thus, those results demonstrate that cobalt and selenium were successfully synthesized with 1:2 of stoichiometry by hydrothermal method.

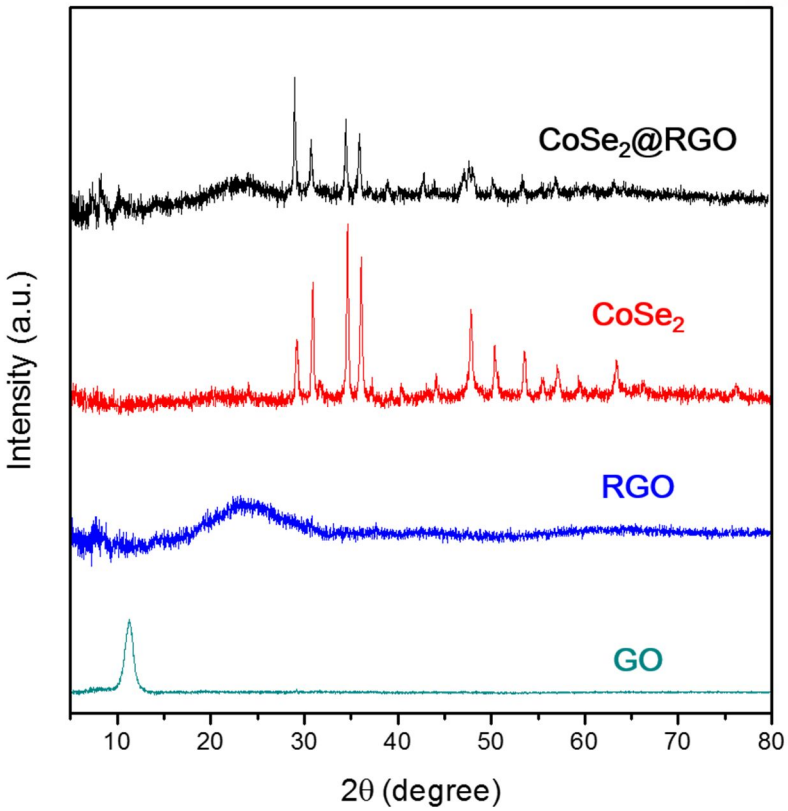

<Figure 14> X-ray diffraction patterns of $CoSe_2$@RGO, $CoSe_2$, RGO and GO.

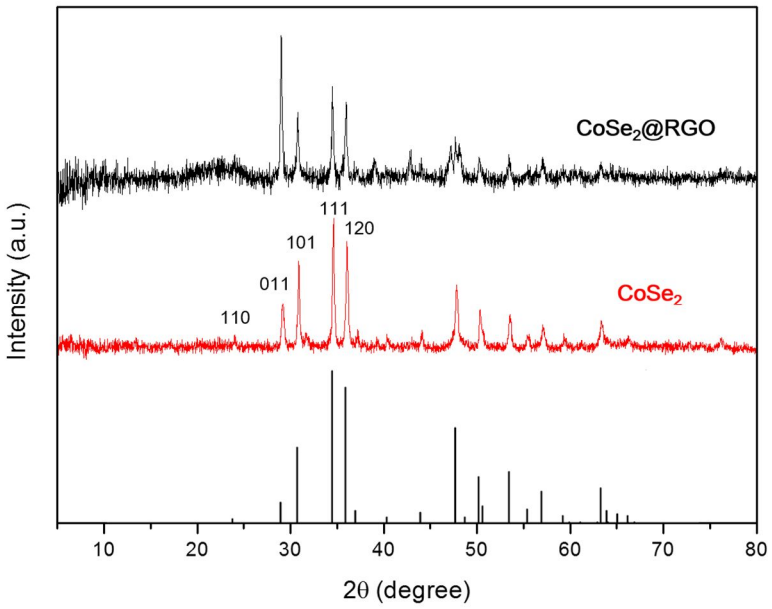

<Figure 15> Comparison of as-prepared $CoSe_2$ compound samples with the standard data of orthorhombic $CoSe_2$ (the perpendicularly aligned peaks onto *x*-axis).

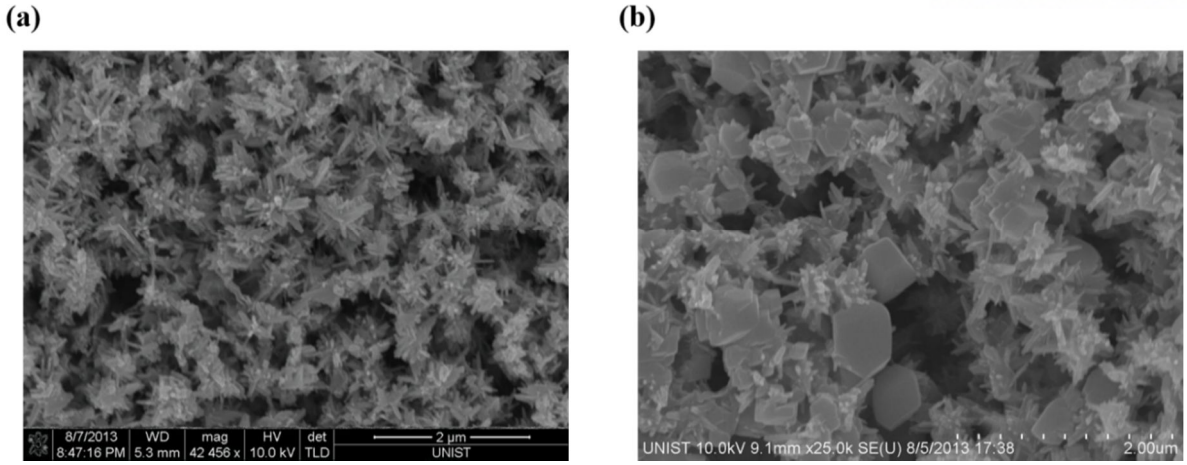

<Figure 16> Scanning electron microscope images of hydrothermally synthesized (a) $CoSe_2$ and (b) $CoSe_2$ and RGO composites.

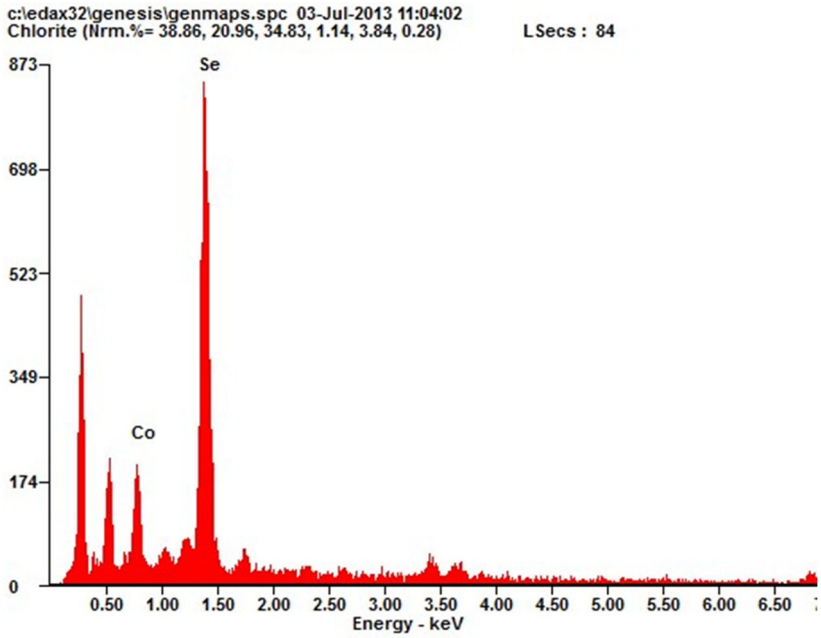

<Figure 17> Energy-dispersive spectroscopy result of $CoSe_2$.

Element	Weight percentage (%)	Atomic percentage (%)
Co L	24.37	30.15
Se L	75.63	69.85

<Table 2> Detailed element contents of Co and Se in synthesized cobalt and selenium compounds.

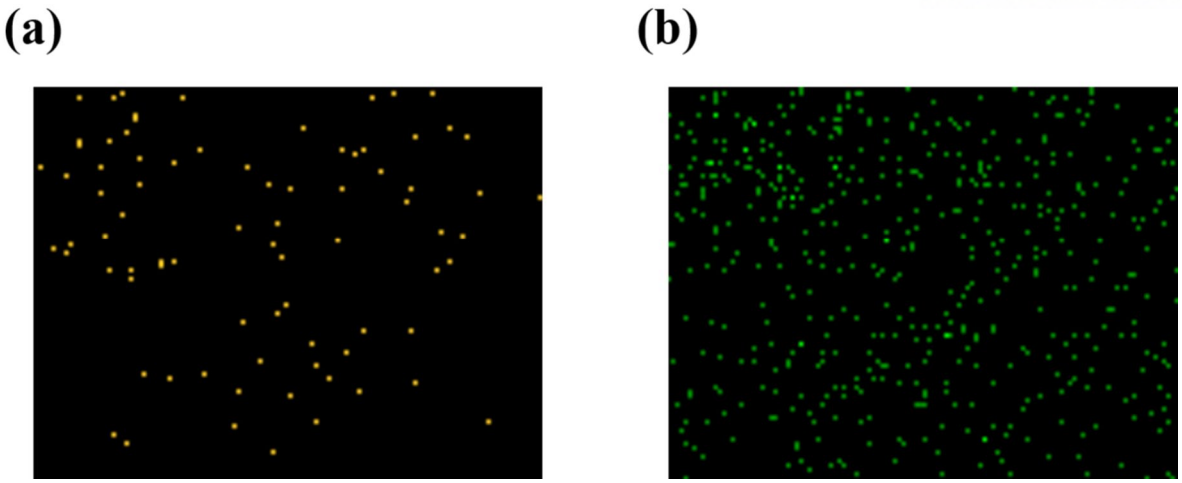

<Figure 18> Distribution of (a) Co and (b) Se atoms in the same area of the $CoSe_2$ specimen.

The Raman spectra of $CoSe_2$ and $CoSe_2$@RGO were shown in Figure 19. The peak at 171 cm^{-1} in $CoSe_2$ and $CoSe_2$@RGO indicates the bending of the Se-Se bonds in the close-packed chains[49]. Unlike pristine $CoSe_2$, the $CoSe_2$@RGO sample contains two peaks at 1328 cm^{-1} and 1587 cm^{-1}. These peaks are known as defect band (D-band, 1328 cm^{-1}) and graphitic band (G-band, 1587 cm^{-1}) which are usually observed in GO and RGO. D-band originates from the presence of some disorder in the graphene structure and G-band is associated with vibration of sp^2-bonded carbon atoms in a two-dimensional hexagonal lattice. Typically, the intensity of D-band to G-band (I_d/I_g) for RGO is higher than that of GO[50], and the same tendency was observed in the $CoSe_2$@RGO sample exhibiting 1.10 of I_d/I_g. Therefore, it can be concluded that GO was converted into RGO after hydrothermal reaction with the formation of $CoSe_2$ compounds.

Figure 20 represents X-ray photoelectron spectroscopy (XPS) peaks of Co 2p and Se 3d for as-synthesized $CoSe_2$ and $CoSe_2$@RGO. The presence of Co peaks and Se peaks could be observed, corresponding to Co $2p_{3/2}$ at 778.5 eV, Co $2p_{1/2}$ at 793.5 eV, Se $3d_{5/2}$ at 54.6 eV, and Se $3d_{3/2}$ at 55.3 eV, respectively. These results are consistent with $CoSe_2$.[51] Figure 21 shows the XPS peaks of C 1s for GO, RGO, $CoSe_2$ and $CoSe_2$@RGO. In the GO sample, there are some peaks associated with the bonds between carbon and oxygen; the two peaks with strong intensity at 284.6 eV for C-C or C=C bond and 286.6 eV for C-O single bond, and the small peak at 287.7 eV for C=O double bond and 288.6 eV for O−C=O bond. However, in cased of RGO, the peaks related with oxygen bond have drastically decreased compared to GO. It indicates that large amount of functional groups related with oxygen has been removed after hydrothermal reaction of GO, being reduced to RGO. The C 1s peaks were also observed in $CoSe_2$ and $CoSe_2$@RGO (it is inevitable for C 1s peaks to be detected in the XPS analysis). However, the C-O peaks at around 286.6 eV in $CoSe_2$@RGO as well as $CoSe_2$ samples

were not strong as the GO sample shows, rather it seemed that only the carbon-carbon peaks exist in both samples. It means that GO in the Co and Se precursor solution was converted to RGO. Moreover, those peaks are not significantly different from each other, but the relative intensity of carbon-carbon bond for $CoSe_2$@RGO is higher than $CoSe_2$, while that of Co and Se is similar to each other. These results suggest that $CoSe_2$@RGO includes carbon derivatives which do not contain a lot of carbon-oxygen bond groups.

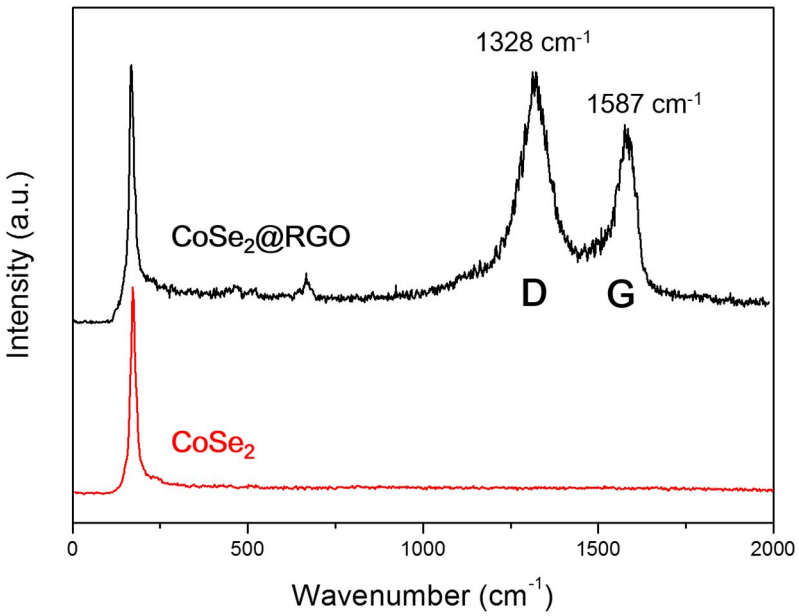

<Figure 19> Raman spectra of $CoSe_2$ and $CoSe_2$@RGO.

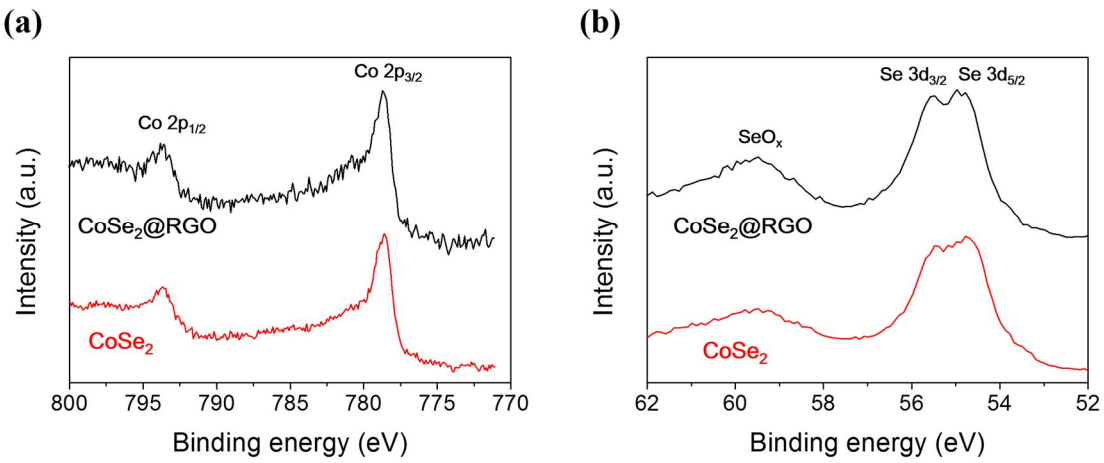

<Figure 20> X-ray photoelectron spectroscopy spectra of Co 2p and Se 3d for $CoSe_2$ and $CoSe_2$@RGO.

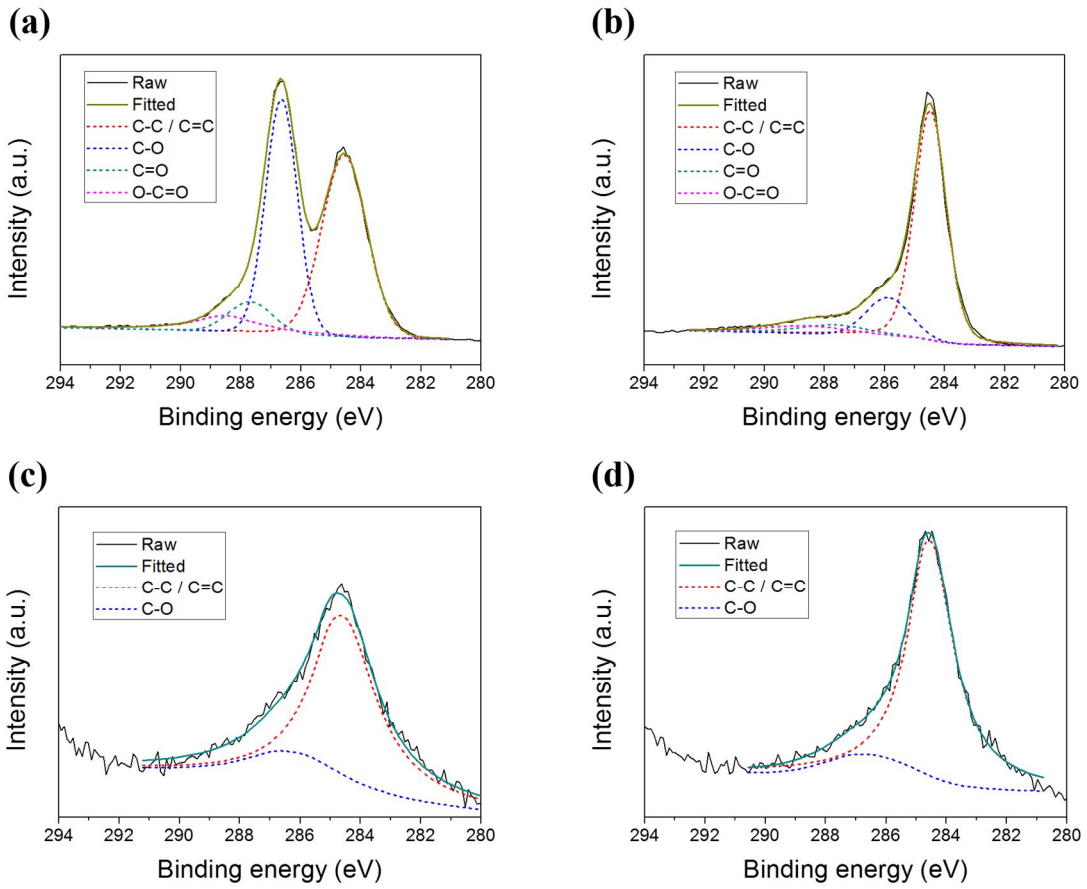

<Figure 21> X-ray photoelectron spectroscopy spectra of C 1s for (a) GO, (b) RGO, (c) $CoSe_2$ and (d) $CoSe_2$@RGO.

3.2. Electrochemical characteristics of counter electrodes

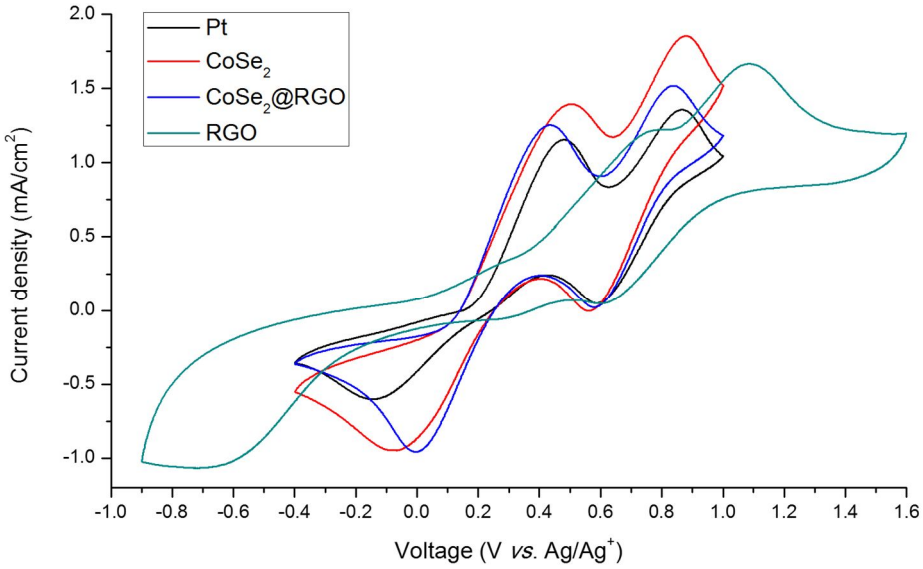

<Figure 22> Cyclic voltammetry curves of iodide/triiodide redox couples for Pt, $CoSe_2$, $CoSe_2$@RGO and RGO counter electrodes.

To interpret catalytic performances of the counter electrodes (CEs), electrochemical analyses of Pt-based and RGO CEs as well as $CoSe_2$ compounds CEs were conducted. The results of three-electrode cyclic voltammetry (CV) of various samples that was measured with a scan rate of 50 mV/s are shown in Figure 22. Two pairs of the peaks corresponding to oxidation and reduction between iodide (I^-) and triiodide (I_3^-) were observed within the range of -0.4 to 1.0 V (vs. Ag/AgCl) for all materials except RGO. The left pair is assigned to Equation 3.2 while the right pair was assigned to Equation 3.3. Also, the positive (anodic) peaks refer to the oxidation of I^- and I_3^-, and the negative (cathodic) peaks are related to the reduction of I^- and I_3^-.

$$I_3^- + 2e^- \leftrightarrow 3I^- \quad (3.2)$$

$$3I_2 + 2e^- \leftrightarrow 2I_3^- \quad (3.3)$$

The differences between the voltages of left pair peaks, also known as the peak-to-peak separation (E_{pp}) of all samples, were examined because it is an important factor to confirm catalytic effects on the CE of DSSCs that is associated with the reduction of I_3^- to I^-. The reduction/oxidation peaks on the left side for Pt, $CoSe_2$ and $CoSe_2$@RGO samples were shown at -0.153 V/0.486 V, -0.077 V/0.508 V and 0.004 V/0.436 V respectively, so each E_{pp} for the reduction of I_3^- to I^- is 0.639 V (Pt), 0.585 V ($CoSe_2$) and 0.432 V ($CoSe_2$@RGO). E_{pp} of RGO CEs could not be confirmed because the peaks

related to the reduction from I_3^- to I^- were not obvious. Because E_{pp} is inversely correlated with the electrochemical rate constant of a redox reaction, the $CoSe_2$@RGO samples which show the lowest E_{pp} value among the samples exhibit better electrocatalytic performances than the others. Moreover, $CoSe_2$ and $CoSe_2$@RGO samples showed higher current density than Pt CEs. It demonstrates that $CoSe_2$ compounds have higher intrinsic catalytic activity than Pt and there is a positive synergetic effect between $CoSe_2$ and RGO for reducing I_3^- to I^-.

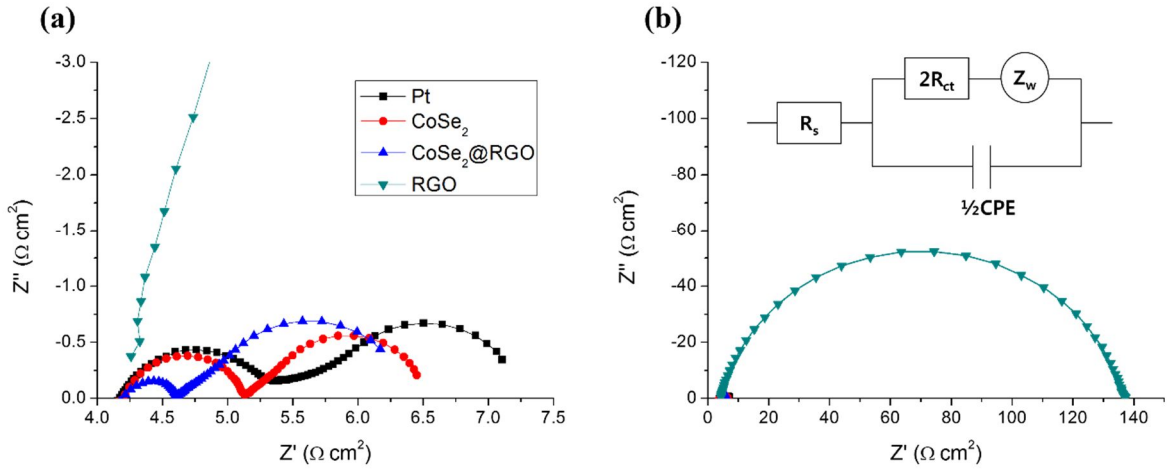

<Figure 23> Nyquist plots of the symmetric dummy cells for (a) Pt, $CoSe_2$, $CoSe_2$@RGO and (b) RGO counter electrodes. The inset in (b) indicates the equivalent circuit of the dummy cells.

	R_{ct} (Ω cm^2)	Z_w (Ω cm^2)
Pt	0.61	1.90
$CoSe_2$	0.50	1.36
$CoSe_2$@RGO	0.20	1.75
RGO	64.75	3.12

<Table 3> The charge transfer resistance and the Nernst diffusion impedance for Pt, $CoSe_2$ and $CoSe_2$@RGO dummy cells. The values were calculated by using the Z-view software.

Electrochemical impedance spectroscopy (EIS) measurement was performed to determine interfacial electrochemical properties, using symmetric dummy cells fabricated with two CEs and iodide liquid electrolyte within the range of 10^{-1} Hz to 10^{6} Hz. The Nyquist plots of Pt, $CoSe_2$, $CoSe_2$@RGO and RGO CEs are shown in Figure 23. The intercept on the real-axis (Z'-axis) at high-frequency region represents the series resistance (R_s), and the first semicircle of plots means the charge transfer resistance (R_{ct}) between the CEs and the electrolyte. The second semicircle at low-frequency region arises from Nernst diffusion impedance (or Warburg impedance, Z_w) of the diffusion of I^-/I_3^- species within the electrolyte. Those information is shown in the equivalent circuit as the inset of Figure 23. RGO CEs exhibited much higher resistance than the others, indicating that RGO materials have lowest catalytic activity among the samples. The R_{ct} and Z_w values for Pt, $CoSe_2$ $CoSe_2$@RGO and RGO calculated by Z-View program were indicated in Table 3. R_{ct} of the $CoSe_2$@RGO cell was the smallest recording 0.20 Ω cm^2, while that of the $CoSe_2$ and Pt cell was 0.50 Ω cm^2 and 0.61 Ω cm^2, respectively. R_{ct} is directly related to the electrocatalytic effects of materials and the number of catalytic sites. For this reason, $CoSe_2$ has better performances than Pt as a catalyst for the CEs of DSSCs, and RGO with $CoSe_2$ serves more active catalytic sites for I_3^- reduction though RGO itself did not show good catalytic effects. Z_w for the three symmetrical cells increased in the order of $CoSe_2$ (1.36 Ω cm^2) < $CoSe_2$@RGO (1.75 Ω cm^2) < Pt (1.90 Ω cm^2). It means that electrocatalytic activity of $CoSe_2$ is superior to Pt, because Z_w decreases when the diffusion coefficient (D) of I_3^- increases. Meanwhile, the resistance parameters of RGO were significantly higher than the others, implying that RGO has low electrocatalytic activity.

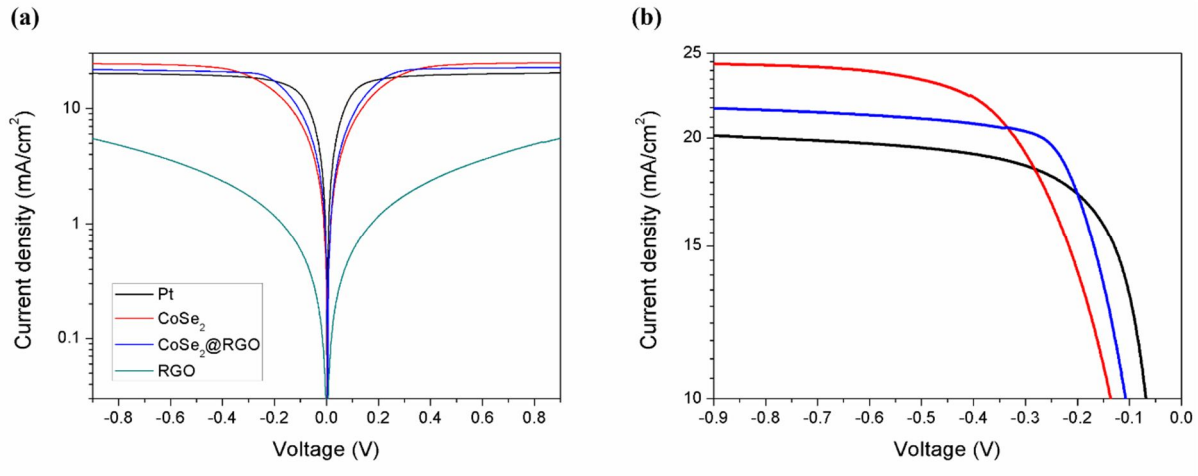

<Figure 24> (a) Tafel polarization curves for Pt, $CoSe_2$, $CoSe_2$@RGO and RGO symmetric cells that are same with the cells used in the EIS measurement and (b) enlarged cathodic branches.

To further elucidate the electrocatalytic activity of various CEs, Tafel polarization analysis was conducted for the symmetric dummy cells used in the EIS experiments. Figure 24 shows the Tafel polarization curves for the symmetric cells based on Pt, $CoSe_2$, $CoSe_2$@RGO and RGO. Theoretically, there are three zones in Tafel curves; the polarization zone at low potential region ($|V| < 0.12$ V), the Tafel zone at the middle potentials with a sharp slope, and the diffusion zone at the high potential zone with a horizontal slope. In the Tafel zone, the intersection of the cathodic branch and the equilibrium potential line can be considered as the exchange current density (J_0). the J_0 can be also calculated by the function of R_{ct}, as described in Equation 3.4.

$$J_0 = \frac{RT}{nFR_{ct}} \tag{3.4}$$

Where R_{ct} is the charge transfer resistance of the CEs, R is the gas constant, T is the absolute temperature, n is the number of electrons involved in the reduction of I_3^- to I^- at the electrode, and F is Faraday's constant.[52] RGO shows both the lowest current density and the gentlest slope, which indicate that RGO has the poorest catalytic activity among the CEs. The slope of the tangent for the anodic or cathodic branches in the Tafel zone was steepest in the $CoSe_2$@RGO CEs, while Pt and $CoSe_2$ exhibited similar slopes. As the slope of the tangent is inversely correlated to R_{ct}, this result is consistent with R_{ct} values in the EIS experiments and RGO helps $CoSe_2$ to reduce I_3^- to I^-. Meanwhile, the intersection of the cathodic branch in the high voltage diffusion zone with the y-axis is defined as the limiting diffusion current density (J_{lim}), which can be expressed with the function of the D, as described in Equation 3.5.

$$J_{lim} = \frac{2nFCD}{l} \tag{3.5}$$

Where n is the electron number involving in the reaction, F is Faraday's constant, l is the spacer thickness, and C is the I_3^- concentration. In can be easily seen that J_{lim} is in the order of Pt < $CoSe_2$@RGO < $CoSe_2$. As J_{lim} varies in direct proportion to D, this result for electrolyte diffusion is consistent with that from the Z_w which was obtained from the EIS analysis.

3.3. Photovoltaic performance of dye-sensitized solar cells

To optimize the performance of solar cells using as-synthesized the composites of $CoSe_2$ with/without RGO, the loading amount of catalyst materials on the substrates was controlled by varying the concentration of precursor dispersion (final loading amount was 10 μg/cm^2, 20 μg/cm^2 and 30 μg/cm^2 on each FTO substrate). The summarized result of photovoltaic parameters according to the loading amount of catalyst materials was indicated in Figure 25. When the loading amount of catalysts was not enough or too much, the photovoltaic performances decreased. Thus, appropriate amount of catalysts is required to generate maximum performance. In this case, the devices which have 20 μg/cm^2 of loading amount mostly exhibited better photovoltaic performances than the others.

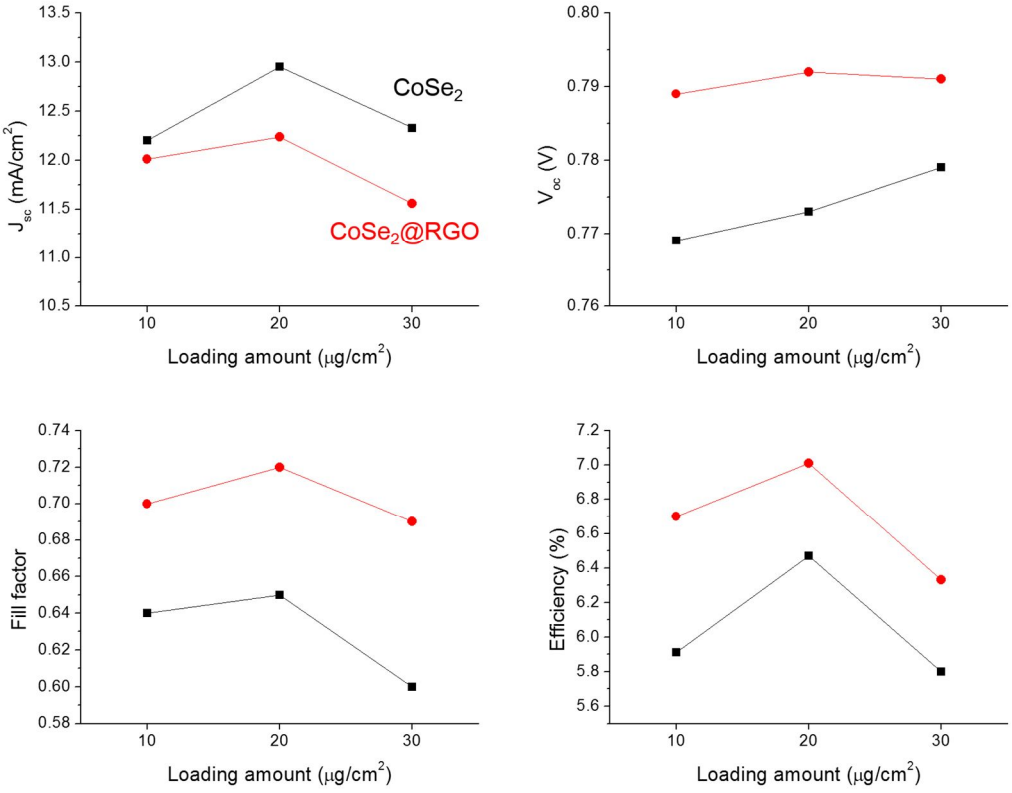

<Figure 25> Photovoltaic parameters for dye-sensitized solar cells using the composites of $CoSe_2$ with/without RGO according to the loading amount.

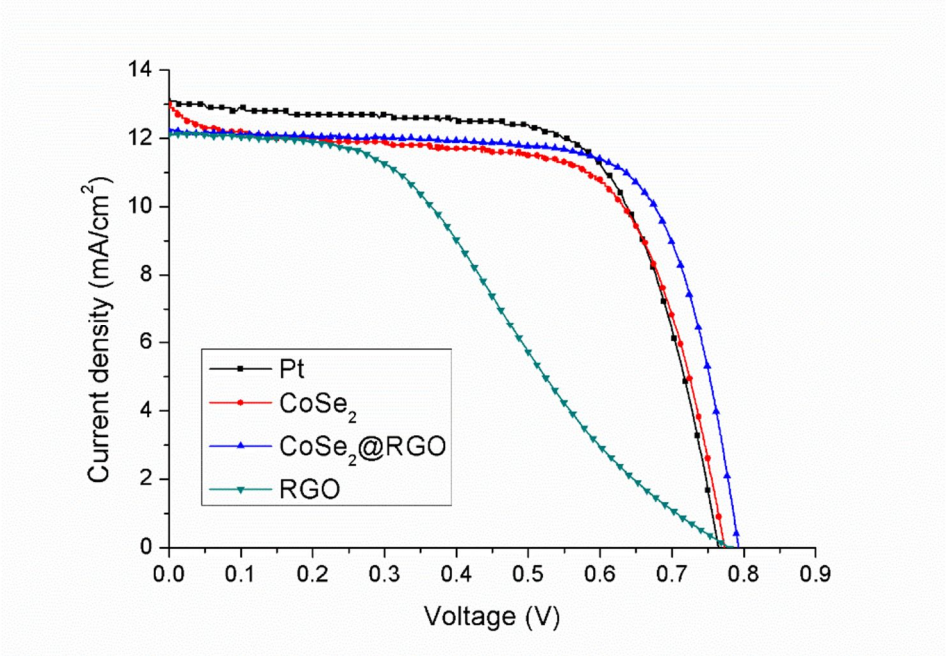

<Figure 26> Current-voltage characteristics of dye-sensitized solar cells with different counter electrodes under simulated AM 1.5G sunlight (100 mW/cm^2).

Counter electrodes	J_{sc} (mA/cm^2)	V_{oc} (V)	FF	Efficiency (%)
Pt	13.12	0.765	0.67	6.77
$CoSe_2$	12.95	0.773	0.65	6.47
$CoSe_2$@RGO	12.24	0.792	0.72	7.01
RGO	12.11	0.761	0.40	3.66

<Table 4> Photovoltaic parameters of dye-sensitized solar cells with different counter electrodes. The loading amount of counter electrode materials on the substrate was fixed to 20 μg/cm^2.

Figure 26 shows the current-voltage (*J-V*) curves of dye-sensitized solar cells (DSSCs) using various counter electrodes (CEs) measured under simulated AM 1.5G sunlight solar simulator, and their photovoltaic parameters were summarized in Table 4. In this experiment, the loading amount of catalyst materials was fixed to 20 μg/cm^2 on the substrate to compare exact effects using the same amount of catalysts. Due to high charge transfer resistance (R_{ct}), RGO CE cells exhibited the lowest performance among the devices, recording comparable J_{sc} (12.11 mA/cm^2) and open-circuit voltage (V_{oc}, 0.761 V) but low fill factor (FF, 0.40) and efficiency (η, 3.66%). Meanwhile, the DSSCs with the $CoSe_2$ CE showed better performances (J_{sc} = 12.95 mA/cm^2, V_{oc} = 0.773 V, FF = 0.65, and η = 6.47%)

that that with the RGO CE. Interestingly, the composites of $CoSe_2$ and RGO exhibited higher efficiency (7.01%) with higher V_{oc} (0.792 V) and FF (0.72) than each component of $CoSe_2$@RGO composites, even also higher than the devices based on the Pt CE (J_{sc} = 13.12 mA/cm^2, V_{oc} = 0.765 V, FF = 0.67 and η = 6.77%), though J_{sc} (12.24 mA/cm^2) was lower than that of Pt CE and $CoSe_2$ CE cells. These improved parameters were attributed to superior electrocatalytic activity (smaller R_{ct}) of the $CoSe_2$@RGO CE. This result suggests that the composites of $CoSe_2$ with RGO can be promising alternatives to the rare metal Pt as the electrocatalyst materials in a CE of DSSCs.

4. Conclusion

In summary, the composites of cobalt diselenide ($CoSe_2$) with reduced graphene oxide (RGO) have been successfully synthesized by a facile hydrothermal reaction of cobalt and selenide ions, and graphene oxide (GO). The formation of $CoSe_2$ compounds and the reduction of GO were confirmed by FE-SEM, EDS, XRD, XPS and Raman analysis. To characterize electrocatalytic activity of $CoSe_2$ derivatives as the catalysts for a counter electrode (CE) of dye-sensitized solar cells (DSSCs), electrochemical analyses such as EIS, CV and Tafel polarization were carried out. Those analyses demonstrated that $CoSe_2$@RGO has excellent electrocatalytic effects for reduction of triiodide (I_3^-) due to its low charge transfer resistance (R_{ct}), recording 0.20 Ω cm^2 which is lower than that of Pt (0.61 Ω cm^2). DSSCs using the $CoSe_2$@RGO catalysts exhibited higher power conversion efficiency (7.01%) than the Pt-based devices (6.77%) under AM 1.5G sunlight illumination. The results in this study indicate that the composites of $CoSe_2$ with RGO are promising materials with low cost and high performance as a catalyst in a CE of DSSCs.

References

1. Holeczek, H., Renewables: Global status report 2014. *Galvanotechnik* **2014,** *105* (9), 2016-2021.

2. Memming, R., PHOTOCHEMICAL AND ELECTROCHEMICAL PROCESSES OF EXCITED DYES AT SEMICONDUCTOR AND METAL ELECTRODES. *Photochemistry and Photobiology* **1972,** *16* (4), 325-333.

3. Matsumura, M.; Nomura, Y.; Tsubomura, H., Dye-sensitization on the photocurrent at zinc oxide electrode in aqueous electrolyte solution. *Bulletin of the Chemical Society of Japan* **1977,** *50* (10), 2533-2537.

4. O'Regan, B.; Grätzel, M., A low-cost, high-efficiency solar cell based on dye-sensitized colloidal TiO_2 films. *Nature* **1991,** *353* (6346), 737-740.

5. Bashar, S. A., Study of indium tin oxide (ITO) for novel optoelectronic devices. *University of London* **1998**.

6. Mehmood, U.; Rahman, S.-u.; Harrabi, K.; Hussein, I. A.; Reddy, B. V. S., Recent Advances in Dye Sensitized Solar Cells. *Advances in Materials Science and Engineering* **2014,** *2014*, 1-12.

7. Cha, S. I.; Kim, Y.; Hwang, K. H.; Shin, Y.-J.; Seo, S. H.; Lee, D. Y., Dye-sensitized solar cells on glass paper: TCO-free highly bendable dye-sensitized solar cells inspired by the traditional Korean door structure. *Energy & Environmental Science* **2012,** *5* (3), 6071.

8. Lee, K. S.; Lee, H. K.; Wang, D. H.; Park, N. G.; Lee, J. Y.; Park, O. O.; Park, J. H., Dye-sensitized solar cells with Pt- and TCO-free counter electrodes. *Chemical communications* **2010,** *46* (25), 4505-7.

9. Ahn, J.; Lee, K. C.; Kim, D.; Lee, C.; Lee, S.; Cho, D. W.; Kyung, S.; Im, C., Synthesis of Novel Ruthenium Dyes with Thiophene or Thienothiophene Substituted Terpyridyl Ligands and Their Characterization. *Molecular Crystals and Liquid Crystals* **2013,** *581* (1), 45-51.

10. Yin, J.-F.; Bhattacharya, D.; Hsu, Y.-C.; Tsai, C.-C.; Lu, K.-L.; Lin, H.-C.; Chen, J.-G.; Ho, K.-C., Enhanced photovoltaic performance by synergism of light-cultivation and electronic localization for highly efficient dye-sensitized solar cells. *Journal of Materials Chemistry* **2009,** *19* (38), 7036.

11. Park, N. G.; Van De Lagemaat, J.; Frank, A. J., Comparison of dye-sensitized rutile- and anatase-based TiO_2 solar cells. *Journal of Physical Chemistry B* **2000,** *104* (38), 8989-8994.

12. Zhang, Q.; Dandeneau, C. S.; Zhou, X.; Cao, G., ZnO Nanostructures for Dye-Sensitized Solar Cells. *Adv Mater* **2009,** *21* (41), 4087-4108.

13. Feng, X. J.; Shankar, K.; Varghese, O. K.; Paulose, M.; Latempa, T. J.; Grimes, C. A., Vertically Aligned Single Crystal TiO_2 Nanowire Arrays Grown Directly on Transparent Conducting Oxide Coated Glass: Synthesis Details and Applications. *Nano Lett* **2008,** *8* (11), 3781-3786.

14. Law, M.; Greene, L. E.; Johnson, J. C.; Saykally, R.; Yang, P., Nanowire dye-sensitized solar cells. *Nature materials* **2005,** *4* (6), 455-9.

15. Kang, S. H.; Choi, S. H.; Kang, M. S.; Kim, J. Y.; Kim, H. S.; Hyeon, T.; Sung, Y. E., Nanorod-Based Dye-Sensitized Solar Cells with Improved Charge Collection Efficiency. *Adv Mater* **2008,** *20* (1), 54-58.

16. Mor, G. K.; Shankar, K.; Paulose, M.; Varghese, O. K.; Grimes, C. A., Use of highly-ordered TiO_2 nanotube arrays in dye-sensitized solar cells. *Nano Lett* **2006,** *6* (2), 215-218.

17. Martinson, A. B. F.; Elam, J. W.; Hupp, J. T.; Pellin, M. J., ZnO nanotube based dye-sensitized solar cells. *Nano letters* **2007,** *7* (8), 2183-2187.

18. Roy, P.; Berger, S.; Schmuki, P., TiO_2 nanotubes: synthesis and applications. *Angewandte Chemie* **2011,** *50* (13), 2904-39.

19. Oh, J.-K.; Lee, J.-K.; Kim, H.-S.; Han, S.-B.; Park, K.-W., TiO_2 Branched Nanostructure Electrodes Synthesized by Seeding Method for Dye-Sensitized Solar Cells. *Chemistry of Materials* **2010,** *22* (3), 1114-1118.

20. Wu, W. Q.; Lei, B. X.; Rao, H. S.; Xu, Y. F.; Wang, Y. F.; Su, C. Y.; Kuang, D. B., Hydrothermal fabrication of hierarchically anatase TiO_2 nanowire arrays on FTO glass for dye-sensitized solar cells. *Scientific reports* **2013,** *3*, 1352.

21. Nazeeruddin, M. K.; Péchy, P.; Renouard, T.; Zakeeruddin, S. M.; Humphry-Baker, R.; Cointe, P.; Liska, P.; Cevey, L.; Costa, E.; Shklover, V.; Spiccia, L.; Deacon, G. B.; Bignozzi, C. A.; Grätzel, M., Engineering of efficient panchromatic sensitizers for nanocrystalline TiO_2-based solar cells. *Journal of the American Chemical Society* **2001,** *123* (8), 1613-1624.

22. Mozer, A. J.; Wagner, P.; Officer, D. L.; Wallace, G. G.; Campbell, W. M.; Miyashita, M.; Sunahara, K.; Mori, S., The origin of open circuit voltage of porphyrin-sensitised TiO_2 solar cells. *Chemical communications* **2008,** (39), 4741-3.

23. Robel, I.; Subramanian, V.; Kuno, M.; Kamat, P. V., Quantum dot solar cells. Harvesting light energy with CdSe nanocrystals molecularly linked to mesoscopic TiO2 films. *Journal of the American Chemical Society* **2006,** *128* (7), 2385-2393.

24. McDonald, S. A.; Konstantatos, G.; Zhang, S.; Cyr, P. W.; Klem, E. J.; Levina, L.; Sargent, E. H., Solution-processed PbS quantum dot infrared photodetectors and photovoltaics. *Nature materials* **2005,** *4* (2), 138-42.

25. Chang, J. A.; Rhee, J. H.; Im, S. H.; Lee, Y. H.; Kim, H. J.; Seok, S. I.; Nazeeruddin, M. K.; Gratzel, M., High-performance nanostructured inorganic-organic heterojunction solar cells. *Nano letters* **2010,** *10* (7), 2609-12.

26. Kojima, A.; Teshima, K.; Shirai, Y.; Miyasaka, T., Organometal halide perovskites as visible-light sensitizers for photovoltaic cells. *Journal of the American Chemical Society* **2009,** *131* (17), 6050-6051.

27. Nazeeruddin, M. K.; Kay, A.; Rodicio, I.; Humphry-Baker, R.; Müller, E.; Liska, P.; Vlachopoulos, N.; Grätzel, M., Conversion of light to electricity by cis-X_2bis(2,2′-bipyridyl-4,4′-dicarboxylate)ruthenium(II) charge-transfer sensitizers (X = Cl^-, Br^-, I^-, CN^-, and SCN^-) on nanocrystalline TiO_2 electrodes. *Journal of the American Chemical Society* **1993,** *115* (14), 6382-6390.

28. Kambe, S.; Nakade, S.; Kitamura, T.; Wada, Y.; Yanagida, S., Influence of the electrolytes on electron transport in mesoporous TiO_2-electrolyte systems. *The Journal of Physical Chemistry B* **2002,** *106* (11), 2967-2972.

29. Yella, A.; Lee, H. W.; Tsao, H. N.; Yi, C.; Chandiran, A. K.; Nazeeruddin, M. K.; Diau, E. W.; Yeh, C. Y.; Zakeeruddin, S. M.; Gratzel, M., Porphyrin-sensitized solar cells with cobalt (II/III)-based redox electrolyte exceed 12 percent efficiency. *Science* **2011,** *334* (6056), 629-34.

30. Gorlov, M.; Kloo, L., Ionic liquid electrolytes for dye-sensitized solar cells. *Dalton Transactions* **2008,** (20), 2655.

31. Wang, P.; Zakeeruddin, S. M.; Grätzel, M., Solidifying liquid electrolytes with fluorine polymer and silica nanoparticles for quasi-solid dye-sensitized solar cells. *Journal of Fluorine Chemistry* **2004,** *125* (8), 1241-1245.

32. Kubo, W.; Kitamura, T.; Hanabusa, K.; Wada, Y.; Yanagida, S., Quasi-solid-state dye-sensitized solar cells using room temperature molten salts and a low molecular weight gelator. *Chemical communications* **2002,** (4), 374-375.

33. Bach, U.; Lupo, D.; Comte, P.; Moser, J. E.; Weissörtel, F.; Salbeck, J.; Spreitzer, H.; Grätzel, M., Solid-state dye-sensitized mesoporous TiO2 solar cells with high photon-to-electron conversion efficiencies. *Nature* **1998,** *395* (6702), 583-585.

34. Papageorgiou, N.; Maier, W. F.; Grätzel, M., An iodine/triiodide reduction electrocatalyst for aqueous and organic media. *Journal of the Electrochemical Society* **1997,** *144* (3), 876-884.

35. Park, J.-G.; Akhtar, M. S.; Li, Z. Y.; Cho, D.-S.; Lee, W.; Yang, O. B., Application of single walled carbon nanotubes as counter electrode for dye sensitized solar cells. *Electrochimica Acta* **2012,** *85*, 600-604.

36. Ramasamy, E.; Chun, J.; Lee, J., Soft-template synthesized ordered mesoporous carbon counter electrodes for dye-sensitized solar cells. *Carbon* **2010,** *48* (15), 4563-4565.

37. Kavan, L.; Yum, J. H.; Grätzel, M., Optically transparent cathode for dye-sensitized solar cells based on graphene nanoplatelets. *ACS Nano* **2011,** *5* (1), 165-172.

38. Wang, M.; Anghel, A. M.; Marsan, B. t.; Cevey Ha, N.-L.; Pootrakulchote, N.; Zakeeruddin, S. M.; Gra tzel, M., CoS Supersedes Pt as Efficient Electrocatalyst for Triiodide Reduction in Dye-Sensitized Solar Cells. *Journal of the American Chemical Society* **2009,** *131* (44), 15976-15977.

39. Wang, Y. C.; Wang, D. Y.; Jiang, Y. T.; Chen, H. A.; Chen, C. C.; Ho, K. C.; Chou, H. L.; Chen, C. W., FeS_2 nanocrystal ink as a catalytic electrode for dye-sensitized solar cells. *Angewandte Chemie* **2013,** *52* (26), 6694-8.

40. Murakami, T. N.; Grätzel, M., Counter electrodes for DSC: Application of functional materials as catalysts. *Inorganica Chimica Acta* **2008,** *361* (3), 572-580.

41. Balasingam, S. K.; Kang, M. G.; Jun, Y., Metal substrate based electrodes for flexible dye-sensitized solar cells: fabrication methods, progress and challenges. *Chemical communications* **2013,** *49* (98), 11457-75.

42. Green, M. A.; Emery, K.; Hishikawa, Y.; Warta, W.; Dunlop, E. D., Solar cell efficiency tables (version 44). *Progress in Photovoltaics: Research and Applications* **2014,** *22* (7), 701-710.

43. Kay, A.; Grätzel, M., Low cost photovoltaic modules based on dye sensitized nanocrystalline titanium dioxide and carbon powder. *Solar Energy Materials and Solar Cells* **1996,** *44* (1), 99-117.

44. Gao, M. R.; Xu, Y. F.; Jiang, J.; Yu, S. H., Nanostructured metal chalcogenides: synthesis, modification, and applications in energy conversion and storage devices. *Chemical Society reviews* **2013,** *42* (7), 2986-3017.

45. Gong, F.; Wang, H.; Xu, X.; Zhou, G.; Wang, Z. S., In situ growth of $Co_{0.85}Se$ and $Ni_{0.85}Se$ on conductive substrates as high-performance counter electrodes for dye-sensitized solar cells. *Journal of the American Chemical Society* **2012,** *134* (26), 10953-8.

46. Gong, F.; Xu, X.; Li, Z.; Zhou, G.; Wang, Z. S., $NiSe_2$ as an efficient electrocatalyst for a Pt-free counter electrode of dye-sensitized solar cells. *Chemical communications* **2013,** *49* (14), 1437-9.

47. Li, Z.; Gong, F.; Zhou, G.; Wang, Z.-S., NiS_2/Reduced Graphene Oxide Nanocomposites for Efficient Dye-Sensitized Solar Cells. *The Journal of Physical Chemistry C* **2013,** *117* (13), 6561-6566.

48. Yang, J.; Cheng, G. H.; Zeng, J. H.; Yu, S. H.; Liu, X. M.; Qian, Y. T., Shape control and characterization of transition metal diselenides MSe_2 (M = Ni, Co, Fe) prepared by a solvothermal-reduction process. *Chemistry of Materials* **2001,** *13* (3), 848-853.

49. Carim, A. I.; Saadi, F. H.; Soriaga, M. P.; Lewis, N. S., Electrocatalysis of the hydrogen-evolution reaction by electrodeposited amorphous cobalt selenide films. *Journal of Materials Chemistry A* **2014,** *2* (34), 13835.

50. Stankovich, S.; Dikin, D. A.; Piner, R. D.; Kohlhaas, K. A.; Kleinhammes, A.; Jia, Y.; Wu, Y.; Nguyen, S. T.; Ruoff, R. S., Synthesis of graphene-based nanosheets via chemical reduction of exfoliated graphite oxide. *Carbon* **2007,** *45* (7), 1558-1565.

51. Kong, D.; Wang, H.; Lu, Z.; Cui, Y., $CoSe_2$ nanoparticles grown on carbon fiber paper: an efficient and stable electrocatalyst for hydrogen evolution reaction. *Journal of the American Chemical Society* **2014,** *136* (13), 4897-900.

52. Wu, M.; Lin, X.; Wang, Y.; Wang, L.; Guo, W.; Qi, D.; Peng, X.; Hagfeldt, A.; Gratzel, M.; Ma, T., Economical Pt-free catalysts for counter electrodes of dye-sensitized solar cells. *Journal of the American Chemical Society* **2012,** *134* (7), 3419-28.

Acknowledgement

생각해보면 대학원에 입학한 지 정말 얼마 되지도 않은 것 같은데, 어느 새 석사 학위 수여를 앞두게 되었습니다. 'Master of Science'. 제가 받게 될 학위의 영어 이름입니다. 다른 뜻으로 직역하면 '과학에 통달한 자' 정도가 됩니다. 하지만 2년 동안 연구 및 실험했던 것들을 돌이켜 보면, 제가 이 거창한 단어에 어울릴 만큼 열심히 했다고는 생각하지 않기 때문에 부끄러운 마음이 듭니다. 그래서 '앞으로는 정말 Master가 되라'는 뜻으로 학위를 받고 더욱 열심히 노력하도록 하겠습니다. 그리고 이 자리를 빌어 제가 'Master' 학위를 받을 수 있게 끔 도와주신 모든 여러분들께 감사 인사를 올리도록 하겠습니다.

그 동안 우리 실험실에 크고 작은 일이 있었지만, 그럼에도 부족한 저를 끝까지 자상하게 이끌어주신 전용석 교수님, 진심으로 감사하고 존경합니다. 교수님께서 가르쳐주신 귀감이 될 만한 모든 것들을 가슴 깊이 새기도록 하겠습니다. 저의 졸업논문 심사에 도움을 주신 홍성유 교수님, 권태혁 교수님께도 깊은 감사를 드립니다.

제가 2년 동안 생사……까지는 아니지만 기쁜 일 궂은 일 같이 했던 모든 Solarinno 랩 인원들 감사합니다. 솔라리노와 수아의 아버지 임현이형, 가장 완벽한 남자 정민이형, 약방의 감초 초롱이누나, 깨알같이 도움 준 재영이형, 너무x10 착한 민오형, 둘도 없는 룸메이트 Suresh, 둘도 없는 동기 성영이, 랩실의 활력소 요한이형, 그리고 윤용주 박사님. 박사님 안 계셨으면 저는 진짜 졸업 못 했을 겁니다. 은혜 잊지 않겠습니다. 이 밖에도 솔라리노를 거쳐가신 모든 졸업생 선배님들, 포스트 닥터, 연구원 여러분들 고맙습니다. 여러분들께서 초석을 잘 다져놓으셨기 때문에 지금의 솔라리노가 있을 수 있었고, 앞으로 더욱 발전할 수 있으리라 생각합니다.

한국기술교육대 응용화학공학과 출신 유니스트 대학원생 선배님들 및 친구들 정말 감사합니다. 대학원 진학에 대한 조언을 구할 수 있었던 선배님들, 함께 있을 수 있어서 큰 의지가 되었던 친구들의 존재는 대학원 생활을 하는 데 있어 정말 큰 힘이 되었습니다.

끝으로, 대학원 진학에 대해 한 치의 반대 없이 저를 믿어주신 가족 여러분들께 감사 드립니다. 대학교, 대학원 모두 타지 생활 한답시고 잘 찾아 뵙지도 않는 못난 아들 뒷바라지 해주신 부모님, 그런 부모님께 잘 효도해드……렸을 것이라 믿는 형, 감사합니다. 여러분들의 믿음이 있었기에 이 자리까지 올 수 있었다고 생각합니다. 반드시 믿음에 보답하도록 하겠습니다.